Results in Materials 10 (2021) 100193

Contents lists available at ScienceDirect

Results in Materials

journal homepage: www.sciencedirect.com/journal/results-in-materials

Tensile stress strain model of polyvinyl chloride/calcium carbonate (PVC/$CaCO_3$) nanocomposite plank

Sary A. Malak

Department of Civil and Environmental Engineering, Notre Dame University, Louaize, Zouk Michael, Zouk Mosbeh, P.O. Box 72, Lebanon

ARTICLE INFO

Keywords:
Ductility
Porosity
Tensile strength
Toughness
Rupture strains
Cementitious
Plastics

ABSTRACT

This paper presents the tensile stress strain model of a recyclable polyvinyl chloride/calcium carbonate (PVC/$CaCO_3$) thermo-formable, fire/water proof resistant, and durable composite mineral plank. The paper presents experimentally obtained material stress-strain properties in direct tension as a function of its parameters including thickness, surface texture and grain alignment. With an increase in thickness from 1 mm (0.039 in.) to 12 mm (0.47 in.) for rough surface texture and parallel grain alignment, tensile and rupture strengths decreased from 27.4 MPa (4.11 ksi) to 14 MPa (2.1 ksi) and from 14 MPa (2.1 ksi) to 6 MPa (0.9 ksi) respectively. Strains at rupture increased from 0.01 to 0.02 while the modulus of elasticity decreased from 23078 MPa (3462 ksi) to 2139 MPa (320.85 ksi). Smoothness of surface texture increased the ultimate and rupture stresses by 16% while rupture strains increased by 45% leading to a more ductile material. Grain orientation perpendicular to the load direction resulted in an 18% reduction in ultimate strength. The paper proposes models for predicting the stress strain relationship including modulus of elasticity, toughness, stress and strain in the proportional, ultimate and rupture states in terms of the material parameters. The developed models are essential for establishing code requirements and design criteria for structural members retrofitted with this type of composite.

1. Introduction

PVC/$CaCO_3$ composite plank is manufactured by mixing PVC plastic resin with calcium carbonate fillers under high temperatures. The material commercial product is called NOVAPLAK (new plank). The material is maintenance free, fire/water resistant, chemical resistant, durable, and 100% recyclable. The material can be used architecturally however from a structural perspective, no information is provided on its mechanical properties including its tensile response. Besides the architectural and environmental benefits, PVC/$CaCO_3$ composites differ from other cementitious and polymer composites used in the construction industry in the following aspects: a) it can be a multi-use fire rated formwork sheet that does not need a release agent and offers the possibility of texturing the concrete surface b). it can be thermo-formable by bending and welding through heating thus easier to construct in the field. c). its mechanical properties can be varied by varying its different parameters including thickness, grain alignment and surface texture based on structural applicability and design requirements. d). its ease of prefabrication in the shop is adaptable to producing different shapes and sizes as required for structural use.

Extensive research has been developed focusing on the tensile mechanical properties of similar types of plastic/$CaCO_3$ composites through experimental investigations. However no tensile stress strain models are available to predict the tensile response as a function of its thickness, grain alignment, and surface texture. The following section summarizes some of the existing findings with respect to the experimental and analytical tensile mechanical properties of similar plastic/filler composites.

1.1. Experimental investigation background

1.1.1. Polyvinyl chloride (PVC)/$CaCO_3$ composites

Studies [1] were developed to show the effect of nano-precipitated or synthetic calcium carbonate (NPCC) on the mechanical properties of unplasticized PVC and acrylic unplasticized PVC. The effect of NPCC on the matrix showed a decrease in the tensile strength from 55 MPa (8.25 ksi) to 45 MPa (6.75 ksi) for PVC and 40 MPa (6 ksi) to 30 MPa (4.5 ksi) for acrylic PVC for a range of NPCC between 0 and 20 parts per hundred parts of resin (phr).

Tensile tests were performed [2] on 200 mm × 80 mm x 3.2 mm (7.8 in. × 3.1 in. x 0.13 in.) composite plates consisting of PVC/$CaCO_3$ composites. The composites were formed through mixing in a high speed

E-mail address: smalak@ndu.edu.lb.

https://doi.org/10.1016/j.rinma.2021.100193
Received in revised form 15 April 2021; Accepted 25 April 2021
Available online 18 May 2021

mixer and then plasticized by a roll mill at 180 °C (356 °F). Tensile stresses were in the range of 45 MPa (6.75 ksi) and young's modulus at 1200 MPa (180 ksi) for different amounts of filler. Rupture stains were at 0.45 for a 5 wt% (percent by weight) of filler content.

Other studies [3] compared the effect of $CaCO_3$ fillers on typical PVC and PVC blendex blend copolymerized with butadiene 70 wt%, styrene and acrylonitrile. The studies showed that based on a range of filler content between 0 and 25 phr, a reduction of 30% in the tensile strengths and rupture strains was noted when comparing blendex types of PVC to typical PVC composites.

The interfacial adhesion between $CaCO_3$ fillers and PVC was studied [4–7] to show that the surface treatment of the filler with silane coupling agents as well as polymethyl methacrylate (PMMA) improved the tensile strength, modulus of elasticity and rupture strains of the composite. Different filler sizes were also investigated indicating that the finer the filler the better the formation of a good interface layer is formed. Tensile stress were in the range of 40 MPa (6 ksi), with rupture stains of 0.05 and young's modulus of 2800 MPa (420 ksi) for treated composites.

Additional studies [8] concluded that $CaCO_3$ containing epoxy gave better mechanical as well as dielectric properties among other $CaCO_3$ loadings. This improvement in mechanical properties is due to the interaction between the molecules enhanced by the reaction between PVC molecules and epoxy with $CaCO_3$ fillers.

PVC based composites were prepared by blending with nano-silica dioxide (SiO_2) which were treated with dimethyl dichlorosilane (DDS) and γ-methylacryloxypropyl trimethoxy (KHS) [10]. Based on an increase in filler quantity from 0 to 8 wt%, the tensile strengths were in the range of 53.5 MPa (8.0 ksi) for untreated fillers. KHS treatment increased the tensile strength to 55.5 MPa (8.3 ksi) while DDS treatment increased it to 54.5 MPa (8.2 ksi).

1.1.2. Polypropylene (PP)/$CaCO_3$ composites

The choice of the processing technique [10] has some influence on the properties of the composite. The extrusion technique and the presence of compatibilisers prepared via mixing was found to be more effective to disperse the fillers ($CaCO_3$) when its concentration is high resulting in better tensile strength.

Additional studies [11] for PP filled with calcium carbonate manufactured through an irradiation polymerization process, noted that the tensile modulus of elasticity remained constant at 1000 MPa (150 ksi) up to 1 wt% of filler content and then increased by 100% to 2000 MPa (300 ksi) for 1.5 wt% of filler content. Tensile strengths remained constant at 35 MPa (5.25 ksi) up to 1 wt% filler content and then were reduced by 30% to 25 MPa (3.75 ksi) for higher filler percentages.

A study [12] was performed to understand the effect of different types of fillers on the mechanical properties of PP. Different fillers were used including talc, kaolin, and calcium carbonate. Talc and kaolin are clay minerals with different hardness and mean particle diameter. The results showed that, in most cases, the strength and stiffness of talc filled PP composite was significantly higher than those of calcium carbonates and kaolin filled PP. However calcium carbonate increased the toughness of the composite. The study showed that for calcium carbonate filled PP, the tensile strengths remained at 16 MPa (2.4 ksi) and the tensile modulus of elasticity increased from 1000 MPa (150 ksi) to 1700 MPa (255 ksi) for an increase of 16 wt% of amount of filler. The rupture strains decreased from 0.5 to 0.2 while rupture stresses increased from 3.1 MPa (0.465 ksi) to 3.4 MPa (0.51 ksi) for the same percent increase of amount of filler.

Another study [13] focusing on the experimental tensile stress stain curves for PP with calcium carbonates showed very contradictory results compared to the previous study [12]. The ultimate tensile strengths are in the range of 35 MPa (5.25 ksi) at ultimate strains of 0.1 while rupture stresses were at 25 MPa (3.75 ksi) at strains of 0.2 for 10 wt% of amount of filler. The value for the elastic modulus was in the range of 2500 MPa (375 ksi). The elastic modulus showed a slight increase while the ultimate and rupture stresses showed a slight decrease with an increase in content of calcium carbonates. This variation in the results of the tensile response is a function of the filler surface contact and their dispersion. The toughening effect of the fillers involved basically three aspects: stress concentration, debonding formation or shear bands. Debonding stresses take place before ultimate at values of strains of 0.01 leading to a reduction in the slope of the stress strain curves.

The effect of different mineral fillers on the mechanical properties of PP were investigated including dolomite, mica and wollastonite [14]. Square plates 100 mm × 100 mm x 2.55 mm (3.93 in. × 3.93 in. x 0.1 in.) were fabricated by the injection moulding. The mica filler showed the highest modulus of elasticity compared to wollastonite and dolomite respectively with values increasing from 2000 MPa (300 ksi) to 7000 MPa (1050 ksi) up to 50 wt% of filler content. The tensile strength did not vary much with filler type however a decrease in strength was noted for dolomite from 35 MPa (5.25 ksi) to 18 MPa (2.7 ksi) for an increase in 60 wt% of filler content. Additional tests were performed on surface treatment of dolomite with stearic acid and coupling of titanate showing slight improvement in tensile strength and modulus of elasticity for treated and coupled fillers.

Treated or untreated silica sand or silica dioxide SiO_2 was another replacement to $CaCO_3$ in PP composites [15]. The tensile tests showed that for this type of filler the young's modulus and tensile strength increased with filler content up to 2.5 wt% reaching values of 1200 MPa (180 ksi) and 38 MPa (5.7 ksi) respectively. However for rupture strains and toughness the values increased up to filler content of 1.5 wt% and then decreased for higher percentage of filler content. Rupture strains and toughness reached values of 1 and 20 MPa (3 ksi) for ethyl acrylate treatment of silica sand. It was also noted that the tensile modulus of elasticity and strength increased with the increase of the cross head speed of the testing machine while the strain and toughness decreased.

1.1.3. High density polyethylene (HDPE)/$CaCO_3$ composites

The performance of fillers as a reinforcement is often attributed to the particle size and content. For recycled HDPE with percentages ranging from 60 wt% to 100 wt% (i.e. 0 to 40 wt% fillers) [16], the tensile strengths tend to increase by 18% reaching values up to 32 MPa (4.8 ksi) while moduli of elasticity increased by 90% with values of 1800 MPa (270 ksi). For particles with size less than 0.025 mm (0.00098 in.), no effect on the tensile properties of the HDPE blend was noted.

Other studies [17] considered the use of different calcium carbonate fillers on HDPE matrix based on mean size, size distribution and shape of particles. The study was based on particle density of 2.7 g/cm^3 (0.097 lbs/in.^{3}) with mean sizes ranging between 0.00044 mm (1.7×10^{-5} in.) to 0.0035 mm (1.3×10^{-4} in.) and surface areas per weight in the range between 3×10^6 mm^2/g (600×10^5 in.^{2}/lbs) and 7×10^6 mm^2/g (1350×10^5 in.^{2}/lbs). The percentages for each filler size varied between 0 and 30 wt% resulting in a decrease in values of ultimate strengths from 24.9 MPa (3.74 ksi) to19 MPa (2.85 ksi) at ultimate strains between 0.1 and 0.03. Rupture stresses decreased in values from 14 MPa (2.1 ksi) to 11 MPa (1.65 ksi) with rupture strains ranging between 0.73 and 0.05. Modulus of elasticity ranged in values between 756.1 MPa (113.4 ksi) and 1800 MPa (270 ksi). It was noted that the stress and strains decreased with an increase in the filler content for all the different types of fillers while the modulus of elasticity increased with filler content. For the same filler content, as the mean size of the filler particles decreased, the surface area increased and ultimate stress/strains, rupture stresses/strains and toughness increased while the modulus of elasticity decreased.

1.1.4. Rubber/$CaCO_3$ composites

In the study of rubber/CaCO3 composites [18–20], the tensile properties including tensile strength, modulus of elasticity and rupture stain increase with an increase in the filler content. For an increase of 10 phr filler content, the modulus of elasticity increases from 1500 MPa (225 ksi) to 1850 MPa (278 ksi) while the tensile strength increases from 10 MPa (1.5 ksi) to 16 MPa, (2.4 ksi) and the rupture strain increases

from 6.3 to 7.5 respectively.

1.1.5. Polybutylene succinate (PBS)/$CaCO_3$ composites

In the testing of PBS/CaCO3 [21], the filler dosage was increased from 0 to 30 wt% with a fixed amount of coupling agent of aluminum, titanate and silane at 2 wt%. The tensile strength decreased from 42 MPa (6.3 ksi) to 20 MPa (3 ksi) while the rupture strain increased from 0.5 to 1.1. Additional tests for 30 wt% filler content and a variation of the coupling agent from 1 wt% to 3 wt% produced an increase in tensile strength from 16 MPa (2.4 ksi) to 25 MPa (3.75 ksi) and an increase in rupture strain from 0.17 to 0.25.

1.1.6. Kenaf/polyester Hybrid/$CaCO_3$ composites

Other literature [22] focused on the effect of calcium carbonate on kenaf/polyester hybrid composites. Kenaf is a plant used as a polymer in natural fiber composites. The composite was fabricated with a hand layup method placed in molds and cured at room temperature. Calcium carbonate particles were added in percentages from 2.5 wt% up to 20 wt %. For 80 wt% polyester, 15 wt% kenaf fiber and 5 wt% of fillers, the largest increase in tensile strength of 78% was noted reaching values of 43 MPa (6.45 ksi) was noted. At concentrations of 80 wt% polyester and 20 wt% fillers, the increase of filler percentage led to the formation of bigger agglomerates resulting in a weak interaction between the filler and the matrix. This weak interface resulted in 40% decrease in tensile strengths with values of 25 MPa (3.75 ksi).

1.1.7. Wood/plastic/$CaCO_3$ composites

Studies [23] included the effect of fillers on polyester matrices. The product was prepared by mixing polyethylene (PE) chips with wood flour and calcium carbonates. The product was manufactured by an extruder with a mixing barrel under a heated temperature ranging between 105 °C (222 °F) to 175 °C (347 °F). Increases in tensile strengths of 14% reaching values of 20 MPa (3 ksi) were noted with an increase of up to 30 wt% of filler content and 35 wt% for each of wood flour and polyester. Strains at rupture were also increased by 50% with values up to 0.06 for the same increase in percentage of filler content. It was concluded that 20 wt% of fillers were required to facilitate the processing of the composite, and about 25 wt% of filler was required for optimal tensile response performance.

1.1.8. Polyamide 6 (PA6)/$CaCO_3$ composites

Three different types of CaCO3 were incorporated into PA6 resin at different contents of 5 wt%, 10 wt% and 20 wt% using a corotating twin screw extruder [24]. The types included nanosize–NPCC, precipitated microsize-PCC, and natural occurring microsize-NCC. The increase in dosage content of the filler did not significantly affect either the tensile modulus nor the strength. The NCC filler showed the highest tensile strength at 75 MPa (11.25 ksi) for 5 wt% and 10 wt% filler content similar to the PCC at 20 wt%. The tensile modulus at 3500 MPa (525 ksi) was the highest for PCC at 20 wt% content.

1.1.9. Polyurethane (PU)/$CaCO_3$ composites

The influence of calcium carbonate on the mechanical properties of PU composites formed by rotational molding which is one of the most recent used technologies for the development of larger sized prototypes [25]. Filler increase from 0 to 20 wt% decreased the tensile strength from 16 MPa (2.4 ksi) to 13 MPa (1.95 ksi), the modulus of elasticity increased from 960 MPa (144 ksi) to 1070 MPa (161 ksi) and the rupture stain decreased from 0.03 to 0.016.

1.1.10. Poly(L-lactic acid)(PLLA)/polycaprolactone(PCL)/$CaCO_3$ composites

Tensile stress strain curves were developed for different percentages by weight of PCL weight fraction at different testing rates for PLLA/PCL composites [26]. However no models were developed. PCL is one of the biodegradable polymeric materials widely used for production of bags, sacks and food packaging. The filler content was maintained at 3 wt%. For an increase in PCL weight fraction from 0 to 100 wt%, the modulus of elasticity decreased from 5500 MPa (82.5 ksi) to 500 MPa (75 ksi), the tensile strength decreased from 70 MPa (10.5 ksi) to 16 MPa (2.4 ksi), the rupture stress decreased from 70 MPa (10.5 ksi) to 16 MPa (24 ksi). The rupture strains remained very low up to 60 wt% PCL and increased sharply for higher PCL percentages similar to a percolation phenomenon with a brittle-ductile transition. The rate of loading did not affect significantly the mechanical properties except for the rupture stress at 60 wt% PCL weight were a low rate of testing decreased the rupture stress to 10 MPa (1.5 ksi).

1.2. Analytical modeling background

Some empirical equations for the tensile strength and the modulus of elasticity for PVC/$CaCO_3$ composites were developed as a function of the percentage of filler [2]. The equations were based on the Guth's equation [27] as follows

$$E_c = E_m\left(1 + 2.5\Phi_f + 14.1\Phi_f^2\right) \tag{1}$$

$$\sigma_{yc} = \sigma_{ym}\left(1 - 1.21\Phi_f\right) \tag{2}$$

where E and σ_y are the young's modulus and yield strength, respectively. Subscripts c and m denote composite and matrix, and Φ_f is volume fraction of particles.

Additional equations for the tensile strength for PVC/SiO_2 composites [9] and PP/$CaCO_3$ composites [4,12] were derived based on Pukanzky et al. [28].

$$\sigma_{yc} = \left[\frac{\left(1 - \Phi_f\right)}{\left(1 + 2.5\Phi_f\right)}\right]\sigma_{ym}e^{\left(B\Phi_f\right)} \tag{3}$$

where B is a semi-empirical parameter that accounts for the interface affecting the composite yield. The parameter B reflects the effective interfacial interaction between the inorganic particles and matrix. Jancar and Kucera [29,30] used the B parameter to quantify the interfacial adhesion of PVC/$CaCO_3$ by introducing a relative tensile strength factor Q

$$Q = \left[\frac{\left(1 + 2.5\Phi_f\right)}{\left(1 - \Phi_f\right)}\right]\frac{\sigma_{yc}}{\sigma_{ym}} \tag{4}$$

and B can be obtained by plotting the logarithm of Q versus Φ_f linear dependence. Values of B for untreated, DDS and KHS treatments of PVC/SiO_2 were 3.18, 3.56 and 3.90 respectively [10].

Previous literature [4] indicated that for PVC/$CaCO_3$ composites, values of $B > 3$ imply a strong interfacial adhesion with values for treated particles higher than that for untreated. Values of B for untreated particles ranged between 2.98 and 4.82 while for treated particles from 3.14 to 5.44 depending on the type and fineness of the filler. Literature [12] noted for talc, kaolin, and $CaCO_3$ fillers for PP resin, values of B for the yield stress were at 3.68, 1.89, and 1.44 and for the tensile strength 5.43, 3.99 and 1.12 respectively.

Additional equations for toughness and energy dissipation for PVC/SiO_2 were developed as a function of the filler percentage based on Sumita et al. [31] as follow

$$\frac{E_c''}{E_m''} = \left(1 - b\Phi_f\right)^{-1} \tag{5}$$

where E_c'' and E_m'' represent the loss module of the composite and the pure polymer during the dynamic analyses measurement respectively. The parameter b reflects the interfacial adhesion between the nano-SiO_2 particles and the PVC matrix. The bigger the values of b the stronger the adhesion. b values for untreated, DDS, and KHS particles were 1.66, 3.09 and 3.79 [14].

Other literature for PP/$CaCO_3$ [10,13,14] indicated that equation (1) is only applicable to particles with volume fractions <10% attributed to the formation of network of spherical filler chains [32] based on a volume fraction of spherical fillers

$$\Phi_f = \frac{\rho_c}{\rho_f} W_f \tag{6}$$

where ρ_c is density of composite, ρ_f is density of filler, and W_f is the filler weight fraction. Additional equations for the modulus of elasticity using the law of mixtures [33,34] and Halpin Tsai model equation (7) was presented

$$\frac{E_c}{E_f} = \frac{1 + \xi\eta\Phi_f}{1 - \eta\Psi\Phi_f} \tag{7}$$

$$\Psi = 1 + \left[\frac{(1 - V_{max})}{V_{max}^2}\right]\Phi_f \tag{8}$$

$$\eta = \frac{\left(\frac{E_f}{E_m} - 1\right)}{\left(\frac{E_f}{E_m} + \xi\right)} \tag{9}$$

$$E_c = E_m\Phi_m + E_f\Phi_f \tag{10}$$

$$E_c = \frac{E_m E_f}{(E_m\Phi_m + E_f\Phi_f)} \tag{11}$$

where E_c is the modulus of the composite, E_m and E_f are the moduli of the polymer matrix and filler, $\Phi_m = 1 - \Phi_f$ and Φ_f are the volume fractions of the polymer and filler respectively. ξ is two times the aspect ratio of the filler. V_{max} is maximum packing of the filler = 0.64 for random packing of spherical fillers. Equation (10) is used for strong adhesion between filler and matrix with a larger filler aspect ratio or high surface contact area ($\xi \to \infty$). Equation (11) is the inverse rule of mixtures applicable to rigid spherical particles or low surface contact area ($\xi \to 0$).

For the effect of using flake reinforcement such as mica filler for PP resin [14] and based on Padawar and Beecher [35] the composite modulus of elasticity can be represented as

$$E_c = E_m\Phi_m + E_f\Phi_f MRF \tag{12}$$

where *MRF* is the modulus reduction factor given by

$$MRF = \left(1 - \frac{\tanh(u)}{u}\right) \tag{13}$$

$$u = \alpha\left[\frac{G_m\Phi_f}{E_f(1 - \Phi_f)}\right]^{1/2} \tag{14}$$

where G_m is the shear modulus of the matrix and α is the filler aspect ratio.

Additional equations for the tensile strength for mica, dolomite and wollastonite fillers for PP composites were developed based on Nicolais and Nicodemo [36] as follows

$$\sigma_c = \sigma_m\left(1 - a\Phi_f^b\right) \tag{15}$$

where a is equal to 1 and b is equal to 1 if the material fails by planar fracture and the equation will be similar to equation (2) or b is equal to 2/3 if it fails by random failure [37]. For the case of adhesion between filler and matrix, the empirical equation [37] for tensile strength can be written as

$$\sigma_c = \sigma_m\left(1 - a{\Phi_f}^b + c{\Phi_f}^d\right) \tag{16}$$

where *a, b, c,* and *d* are constants based on an experimental fit of the data.

For HDPE rubber filled particles [38], the empirical equation for the tensile strength was based on equation (15) with the value of a equal to 1 and b equal to 2/3. For rigid particles such as calcium carbonates [17], the tensile strength of composite was based on the development of Hung [39] for a matrix material using the power-law stress/strain connection between the equivalent tensile plastic strain ε_{em} and the equivalent (von Mises) tensile stress σ_{em} of the matrix.

$$\varepsilon_{em} = k{\sigma_{em}}^n \tag{17}$$

The equivalent tensile stress of the composite is related to the tensile stress of the matrix at any equivalent strain level of the matrix by the following equation

$$\frac{\sigma_c(\varepsilon_{em})}{\sigma_{em}(\varepsilon_{em})} = \frac{(1 - \Phi_f)}{(1 - R\Phi_f)} \frac{1}{(1 - \Phi_f)^{1/n}} \tag{18}$$

where $R = R(n)$ is a numerical constant depending on the stress component n of the power law. For HDPE, $n = 3$ giving $R = 1.65$. k is the proportionality constant.

For PLLA/PCL/CaCO3 composites [26], empirical equations for the tensile modulus of elasticity and tensile strength were based on the following equations as a function of the percentage weight fraction of PCL Φ_{PCL}

$$E_c = \alpha_0 + \alpha_1\Phi_{PCL} + \alpha_2{\Phi_{PCL}}^2 \tag{19}$$

$$\sigma_c = \beta_0 + \beta_1\Phi_{PCL} + \beta_2{\Phi_{PCL}}^2 \tag{20}$$

where α_0, α_1, and α_2 are empirical constants based on the stiffness of the composites and β_0, β_1 and β_2 are empirical constants based on the tensile strength of the composite.

In this study, the presented PVC/$CaCO_3$ composite plank contains larger quantities of larger size particles resulting in slightly lower mechanical properties but preserving the rigidity of the composites which is beneficial for retrofit applications. At the same time the material eliminates all the construction-related shortcomings of other cementitious and polymer composites used in the industry and promises to provide a cost-effective long-term repair and retrofit solution that can be readily implemented in the field. Since no stress strain models are present, information on its behavior from a structural standpoint is very limited or nonexistent. Thus, the study will develop experimentally and analytically the tensile response of this material and compares the results with other similar composites. In addition, the tensile stress strain model will be developed to be used for the design of structures retrofitted with this composite.

2. Research significance

The need for a more durable, sustainable, eco-friendly, recyclable, cost-effective composite material for the retrofit and construction of existing building structures led to the development of this material. The material promises improvement in its strength, ductility, constructability effectiveness and energy absorption over other composites. It is essential for long term solutions related to structural improvement.

This research focuses on the development of the tensile stress strain model of PVC/$CaCO_3$ composite as a function of the variables that control it including thickness, grain orientation, and surface texture. There are no stress strain models available in the literature for similar types of composites. The tensile behavior of any material is essential in understanding its structural performance when used as a retrofit solution. For example when it is used simultaneously as permanent formwork and flexural or shear reinforcement in beams and slabs or when it is used as confinement for columns. The tensile stress strain models for PVC/$CaCO_3$ composites has only been recently developed and thus

Fig. 1. Tension specimen.

limited information exist on its tensile behavior. This paper summarizes the experimental observations and compares the results to similar types of composites. From the experimental data, simple analytical models are developed for its tensile stress strain response including modulus of elasticity, elastic stress/strain, ultimate stress/strain, rupture stress/strain and toughness as a function of the material parameters. The paper will be a part of a series of papers on the use of such material in structural retrofit and repair.

3. Experimental investigation

The experimental investigation consisted of uniaxial tensile tests on 50 mm wide x 480 mm long (1.9 in. wide x 18.9 in. long) prisms at different thicknesses ranging between 1 mm (0.039 in.) and 12 mm (0.468 in.). The different thicknesses are 1 mm (0.039 in.), 2 mm (0.078 in.), 3 mm (0.117 in.), 4 mm (0.156 in.), 5 mm (0.195 in.), 6 mm (0.234 in.), 7 mm (0.273 in.), 9 mm (0.351 in.), 10 mm (0.39 in.) and 12 mm (0.468 in.). The samples were cut with the length parallel and perpendicular to the grain direction from prefabricated panels of the required thicknesses. Six samples of each thickness for parallel and perpendicular to the grain were cut totaling 60 samples for each grain direction leading to a total of 120 samples. Additional typical 6 samples of 12 mm (0.468 in.) plywood were tested for grains perpendicular and parallel to the load direction totaling 12 samples for toughness comparison. All samples were based on a typical rough surface texture of the material. For comparing the tensile response between rough and smooth textured materials, additional 6 samples with smooth textured surface were cut for each 3 mm (0.117 in.) and 4 mm (0.156 in.) parallel and perpendicular to the grain totaling 24 specimens.

3.1. Materials

PVC/$CaCO_3$ composite is a mineral composite material manufactured by mixing 67 wt% of powdered recyclable PVC plastic resin with 33 wt% of calcium carbonate ($CaCo_3$) fillers by weight through a heated extruder/calendered (rotating cylinder) concept. The filler enhances the rigidity of the plastic. The PVC resin was obtained from recyclable window and door mullions. The percentage values for the constituents of the composite were based on an optimal processing and tensile response performance. The composite ingredients are mixed with metal oxides including iron oxide (FeO) or titanium dioxide (TiO_2) to produce the required different coloring and pigmentation. The material is manufactured in different shapes mostly planks with different thickness, surface texture and grain alignment. The porosity of the material is a function of its thickness and surface texture which affects the tensile properties.

3.2. Test setup and testing procedure

All specimens were tested using a tensile MATEST machine under a stroke control of 2 mm/min (0.078 in./min) based on ASTM D638 requirements. Tensile specimens were loaded by directly gripping the specimens with axially aligned hydraulic grips. Two linear variable direct transducers (LVDT) were placed on opposite sides of the specimens as shown in Fig. 1. An additional LVDT was placed against the actuator of the test machine to confirm the stroke control rate and displacement.

3.3. Stress strain behavior

All stress-strain curves as shown in Fig. 2 exhibit three main stages:

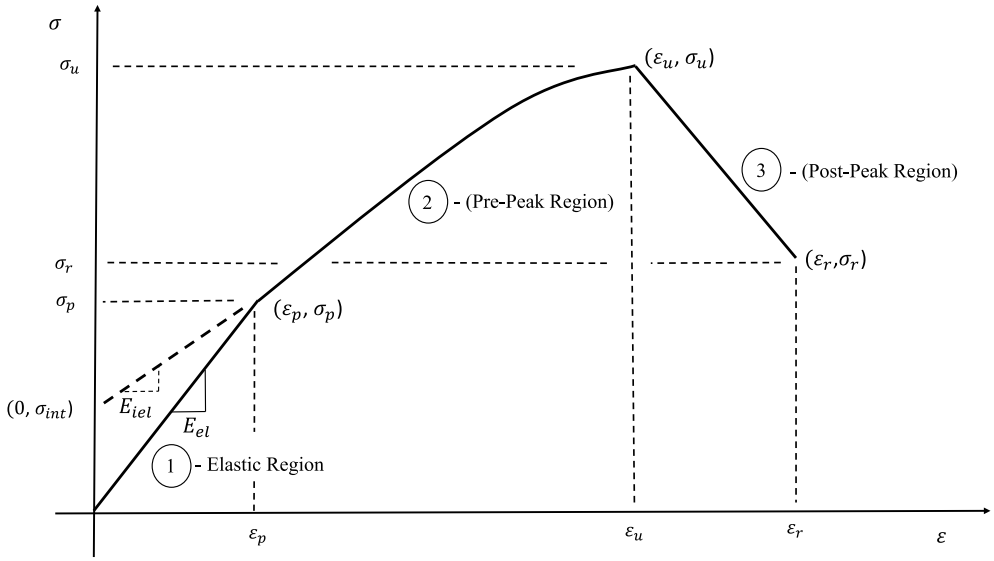

Fig. 2. Typical stress strain response for PVC/CaCO3 composite.

Fig. 3. Localized failure in tension.

- Linear elastic part of the ascending branch which consists of an elastic proportional strain ε_p, elastic proportional stress σ_p, and the slope of the line which represents the elastic modulus of elasticity E_{el},
- In-elastic, i.e. strain hardening part of the ascending branch. This region is a quadratic equation limited by the proportional stress and strain and the ultimate strain ε_u and ultimate stress σ_u. The slope of the curve at the proportional limit is called the inelastic modulus of elasticity E_{iel} and is defined as

$$E_{iel} = \frac{(\sigma_p - \sigma_{int})}{\varepsilon_p} \tag{21}$$

where σ_{int} is the intercept stress obtained by extending the slope line at the proportional limit to the vertical axis. The slope of the curve at the ultimate stress and strain is not equal to zero..

- Linear descending branch limited by the ultimate stress σ_u and strain ε_u and the rupture stress σ_r and rupture strain ε_r. The slopes of the curves are different between the ascending and descending branches at the ultimate state. During the first stage the response was elastic and no cracks were noted were the specimen retains its original shape upon release of load. The second stage is dependent on the porosity (amount of voids) of the material. The porosity is a function of the material thickness and surface texture. For small thicknesses, when the porosity is low, a viscoelastic mechanism is noted where a drop in stress occurs and then again a rise in stress takes place. This is the outcome between stress-increasing of extension and stress-decreasing of relaxation. This behavior results in an increase in strength, durability and impermeability. Mathematical models using homogenized constitutive equations for PP/$CaCO_3$ composites were developed to predict analytically this mechanism in terms of average true stress and true strain. The applicability of the analytic solutions in the entire test range for the ascending portion of the stress strain curve were discussed and improved by experimental results [40]. In this paper, the stress during the viscoelastic region is considered to be the average value of the extension and relaxation stress at a specific strain. As the load approaches the peak value, deformation is localized primarily at a critical crack. When the thickness of the material increases, the porosity increases resulting in a decrease in the viscoelastic mechanism and the drops in the stress values are diminished. Beyond the peak load, a localized failure occurs at a critical crack location as shown in Fig. 3.

3.4. Porosity

Porosity of the material is a major factor that affects the tensile response. It is defined as the amount of voids existing within the thickness of the material. This property is highly dependent on the production heating temperature and the spacing and relative speed of the rotating cylinders during the manufacturing process. Thick materials exhibit higher porosity however by increasing the temperature of production one can maintain lower porosities for thicker materials based on structural demand requirements. Equation (22) represents the porosity as a function of the different properties.

$$p = \frac{C_1 t}{\sigma T E s_f T_e} \tag{22}$$

Table 1
Average values of tensile tests results with rough surface and grain alignment parallel to load direction (1 MPa = 0.15 ksi, 1 mm = 0.039 in.). COV = coefficient of variation.

t mm (in.)	E_{el} MPa (ksi)	σ_p MPa (ksi)	ε_p	σ_u MPa (ksi)	ε_u	σ_{int} MPa (ksi)	E_{iel} MPa (ksi)	σ_r MPa (ksi)	ε_r	T MPa (ksi)	TI
1 (0.039)	23078 (3461.7)	18 (2.7)	0.000898	27.4 (4.11)	0.0104	15.3 (2.29)	2847 (427.05)	14.04 (2.11)	0.0103	0.2263 (0.034)	4.38
2 (0.078)	16164 (2424.6)	11.7 (1.76)	0.001052	21.1 (3.165)	0.012	9.75 (1.46)	2033 (304.95)	9.17 (1.38)	0.0102	0.158 (0.024)	3.063
3 (0.117)	6275 (941.25)	6.4 (0.96)	0.0015	16.1 (2.415)	0.016	3.99 (0.60)	1787 (268.05)	8.51 (1.28)	0.0145	0.142 (0.021)	2.76
4 (0.156)	4416 (662.4)	6.99 (1.05)	0.0015	15.67 (2.351)	0.0127	4.95 (0.74)	1291 (193.65)	7.24 (1.09)	0.0146	0.154 (0.023)	2.99
5 (0.195)	3322 (498.2)	4.64 (0.696)	0.0015	16.7 (2.505)	0.013	2.78 (0.42)	1286 (192.90)	7.98 (1.20)	0.014	0.134 (0.020)	2.6
6 (0.234)	2862 (429.3)	3.95 (0.593)	0.0014	15.2 (2.28)	0.0234	2.58 (0.39)	954 (143.10)	6.64 (1.00)	0.0235	0.215 (0.032)	4.17
7 (0.273)	2484 (372.6)	3.96 (0.594)	0.0015	15.5 (2.325)	0.023	2.90 (0.44)	707 (106.05)	6.8 (1.02)	0.0233	0.213 (0.032)	4.12
9 (0.351)	2249 (337.35)	2.1 (0.315)	0.00096	13.25 (1.988)	0.0175	1.56 (0.23)	553 (82.95)	5.8 (0.87)	0.018	0.124 (0.019)	2.4
10 (0.39)	2434 (365.1)	3.31 (0.497)	0.0015	16.1 (2.415)	0.019	2.34 (0.35)	714 (107.10)	7.1 (1.07)	0.018	0.16 (0.024)	3.13
12 (0.468)	2139 (320.85)	2.75 (0.413)	0.0018	14.03 (2.105)	0.013	1.86 (0.28)	631 (94.65)	6.02 (0.90)	0.016	0.13 (0.020)	2.56
COV	25.4%	15.1%	33.9%	9.5%	24.5%	15.9%	28.8%	9.8%	25.1%	33.1%	33.8%

Table 2
Average values of tensile test results with rough surface and grain alignment perpendicular to load direction (1 MPa = 0.15 ksi, 1 mm = 0.039 in.). COV = coefficient of variation.

t mm (in.)	E_{el} MPa (ksi)	σ_p MPa (ksi)	ε_p	σ_u MPa (ksi)	ε_u	σ_{int} MPa (ksi)	E_{iel} MPa (ksi)	σ_r MPa (ksi)	ε_r	T MPa (ksi)	TI
1 (0.039)	20255 (3038.25)	17.42 (2.61)	0.000743	22 (3.30)	0.00840	14.5 (2.18)	2492 (373.80)	12.6 (1.89)	0.011	0.204 (0.031)	5.39
2 (0.078)	17688 (2653.20)	11.6 (1.74)	0.000943	18.5 (2.78)	0.0121	9.31 (1.40)	1728 (259.20)	7.15 (1.07)	0.0108	0.14 (0.021)	3.28
3 (0.117)	5396 (809.40)	4.83 (0.72)	0.000912	15.4 (2.31)	0.0181	3.66 (0.55)	1202 (180.30)	6.88 (1.03)	0.018	0.17 (0.026)	4.523
4 (0.156)	4474 (671.10)	5.662 (0.85)	0.00134	16.26 (2.44)	0.0215	4.61 (0.69)	1130 (169.50)	7.34 (1.10)	0.0145	0.15 (0.023)	3.97
5 (0.195)	2525 (378.75)	3.72 (0.56)	0.00144	17.31 (2.60)	0.0144	2.324 (0.35)	1101 (165.15)	8.32 (1.25)	0.0196	0.187 (0.028)	3.63
6 (0.234)	3169 (475.35)	3.75 (0.56)	0.00116	14.04 (2.11)	0.0216	2.92 (0.44)	733.8 (110.07)	5.59 (0.84)	0.0182	0.15 (0.023)	3.98
7 (0.273)	2474 (371.10)	3.74 (0.56)	0.00135	13.54 (2.03)	0.021	3.20 (0.48)	423 (63.45)	5.07 (0.76)	0.0243	0.19 (0.029)	5.16
9 (0.351)	1579 (236.85)	2.97 (0.45)	0.00155	14.47 (2.17)	0.0217	1.93 (0.29)	487 (73.05)	5.8 (0.87)	0.0235	0.19 (0.029)	5.19
10 (0.39)	1701 (255.15)	2.73 (0.41)	0.001421	17.1 (2.57)	0.0237	1.245 (0.19)	688 (103.20)	6.9 (1.04)	0.0209	0.16 (0.024)	4.98
12 (0.468)	2405 (360.75)	3.67 (0.55)	0.0013	16.2 (2.43)	0.0174	2.9 (0.44)	615 (92.25)	6.71 (1.01)	0.018	0.16 (0.024)	4.32
COV	22.7%	10.4%	25.5%	6.1%	23.3%	11.8%	31.3%	13.1%	22.1%	17.3%	19.2%

Table 3
Average values of tensile test results with smooth surface and grain alignment parallel to load direction (1 MPa = 0.15 ksi, 1 mm = 0.039 in.). COV = coefficient of variation.

t mm (in.)	E_{el} MPa (ksi)	σ_p MPa (ksi)	ε_p	σ_u MPa (ksi)	ε_u	σ_{int} MPa (ksi)	E_{iel} MPa (ksi)	σ_r MPa (ksi)	ε_r	T MPa (ksi)	TI
3 (0.117)	5275 (791.25)	6.62 (0.99)	0.0016	19.5 (2.93)	0.0194	4.05 (0.61)	2170 (325.50)	8.97 (1.35)	0.023	0.286 (0.04)	5.53
4 (0.156)	4213 (631.95)	8.4 (1.26)	0.002	18.8 (2.82)	0.023	5.04 (0.76)	1683 (252.45)	7.94 (1.19)	0.023	0.3 (0.05)	5.89
COV	36.9%	14.9%	28.6%	6.8%	16.6%	16.4%	25.8%	17.0%	9.6%	12.4%	12.4%

where p represents the porosity, t is the thickness of the material which is a function of the spacing S of the rotating cylinders as defined in equation (23), σ is a generalized stress which is a function of all the different stress states in the tensile response as defined in equation (24), T is the toughness of the material which represents the area under the stress strain curve up to rupture point, E is the generalized modulus of elasticity as a function of the different tensile moduli of elasticity as defined in equation (25), T_e is the heating temperature of the manufacturing process and s_f represents the smoothness factor which is a function of the relative speed V between the rotating cylinders as defined in equation (26). The larger the smoothness factor s_f, the smoother the texture and vise-versa.

$$t = C_2 S \tag{23}$$

$$\sigma = C_3 \sigma_p \sigma_{int} \sigma_u \sigma_r \tag{24}$$

$$E = C_4 E_{el} E_{iel} \tag{25}$$

$$s_f = C_5 V \tag{26}$$

C_1, C_2, C_3, C_4, and C_5 are proportionality constants and all other variables are as defined previously. Equation (22) concludes that an increase in cylinder spacing (increase in thickness) or a decrease in the relative speed of the rotating cylinders (increase in surface texture roughness) or decrease in the manufacturing heating temperature result in higher porosities. High porosities of the material lead to lower stress, toughness and stiffness and higher strains. Porosities are affected more by changes in surface texture than by changes in thickness of the material or changes in the heating temperature of the material production. Further

Table 4
Average values of tensile test results with smooth surface and grain alignment perpendicular to load direction (1 MPa = 0.15 ksi, 1 mm = 0.039 in.). COV = coefficient of variation.

t mm (in.)	E_{el} MPa (ksi)	σ_p MPa (ksi)	ε_p	σ_u MPa (ksi)	ε_u	σ_{int} MPa (ksi)	E_{iel} MPa (ksi)	σ_r MPa (ksi)	ε_r	T MPa (ksi)	TI
3 (0.117)	5443 (816.45)	5.71 (0.86)	0.0012	17.8 (2.67)	0.0181	3.72 (0.56)	1827 (274.05)	8.92 (1.338)	0.021	0.244 (0.037)	6.5
4 (0.156)	4353 (652.95)	6.53 (0.98)	0.0015	18.8 (2.82)	0.0201	5.43 (0.81)	896 (134.4)	8.94 (1.341)	0.022	0.26 (0.039)	7.02
COV	32.3%	16.9%	26.5%	6.6%	16.2%	26.7%	31.4%	9.6%	17.5%	19.7%	19.7%

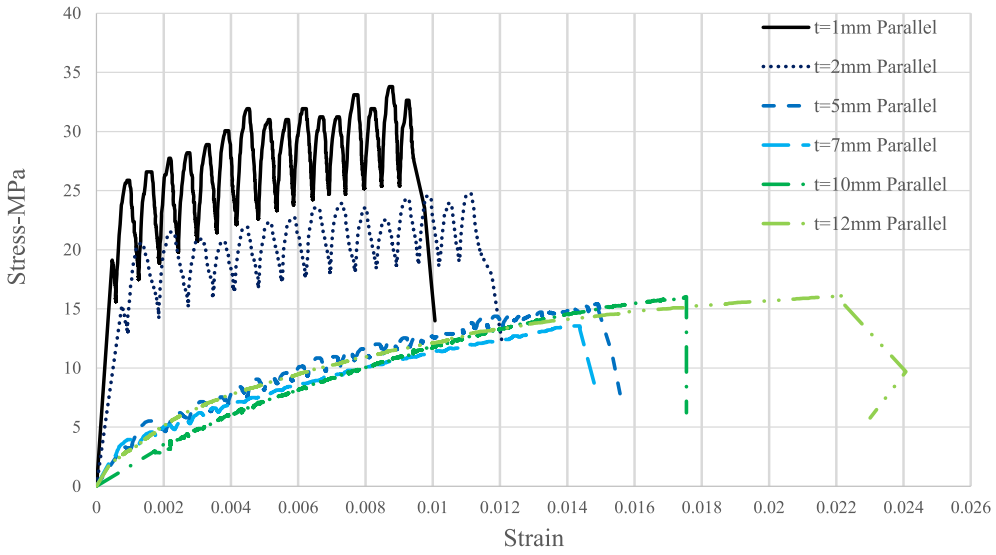

Fig. 4. Typical stress-strain response in tension for grains parallel to load direction. (1 MPa = 0.15 ksi).

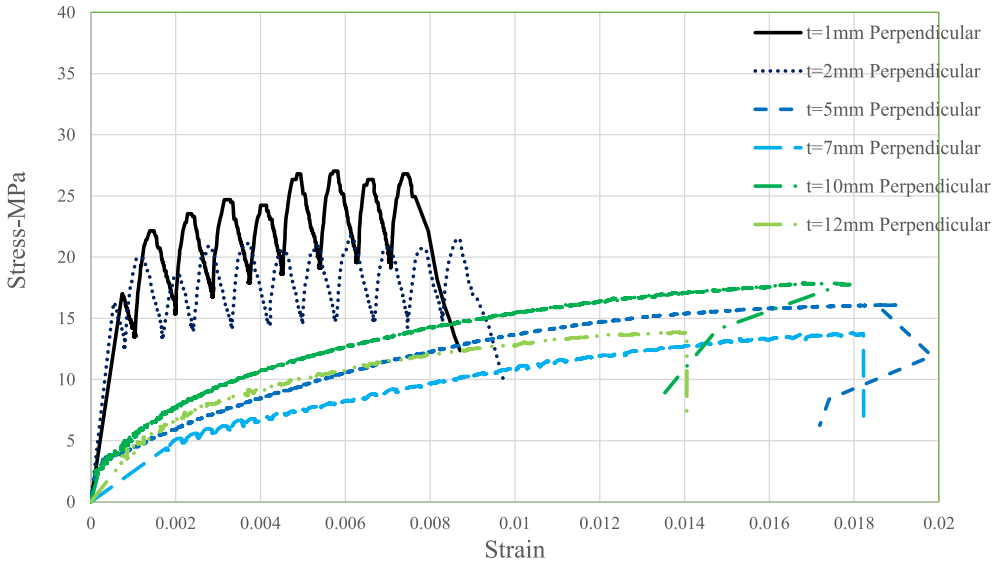

Fig. 5. Typical stress-strain response in tension for grains perpendicular to load direction (1 MPa = 0.15 ksi).

investigation is warranted.

3.5. Experimental results and discussions

Average material properties have been presented in Tables 1 and 2 for rough surface specimens oriented with grains parallel and perpendicular to the load direction respectively. Tables 3 and 4 summarize the average properties for smooth surface specimens with thickness of 3 mm (0.118 in.) and 4 mm (0.157 in.) for grains parallel and perpendicular to the load direction.

All properties in the tables have been defined previously and toughness T of the material is defined as the area under the stress strain curve up to rupture point. The toughness index TI tabulated in the tables for each grain direction is defined as the toughness of the material divided by the toughness of 12 mm (0.47 in.) plywood. Plywood specimens with grains parallel and perpendicular with the load direction were tested as part of this research similar to the testing procedure described herein. The toughness of plywood was obtained at 0.052 MPa (0.0078 ksi) and 0.037 MPa (0.0056 ksi) for grains parallel and perpendicular respectively. The tables of results summarize the coefficient of variation (COV) of the different tensile parameters showing a maximum value of around 35% which is indicative of minimal wide spread scatter beyond the mean values. Figs. 4–8 are representative experimental stress strain curves for different thickness, grain alignment and surface texture. Discussions will focus on ultimate stress and strain, elastic modulus, rupture strain and toughness which represent the strength, stiffness, ductility and energy absorption of the material respectively. In addition, results will be compared to similar composites discussed in the literature review.

3.5.1. Tensile modulus of elasticity

- The inelastic E_{iel} and elastic moduli E_{el} decrease with an increase in thickness due to the increase in porosity of the material. For grains aligned with the load direction, the inelastic modulus decreased from 2847 MPa (427 ksi) to 631 MPa (95 ksi) while the elastic modulus decreased from 23078 MPa (3462 ksi) to 2139 MPa (320.85 ksi) for thicknesses ranging between 1 mm (0.039 in.) and 12 mm (0.47 in.).
- For grains perpendicular to the load direction, the values for the elastic and inelastic moduli averaged almost the same values as for

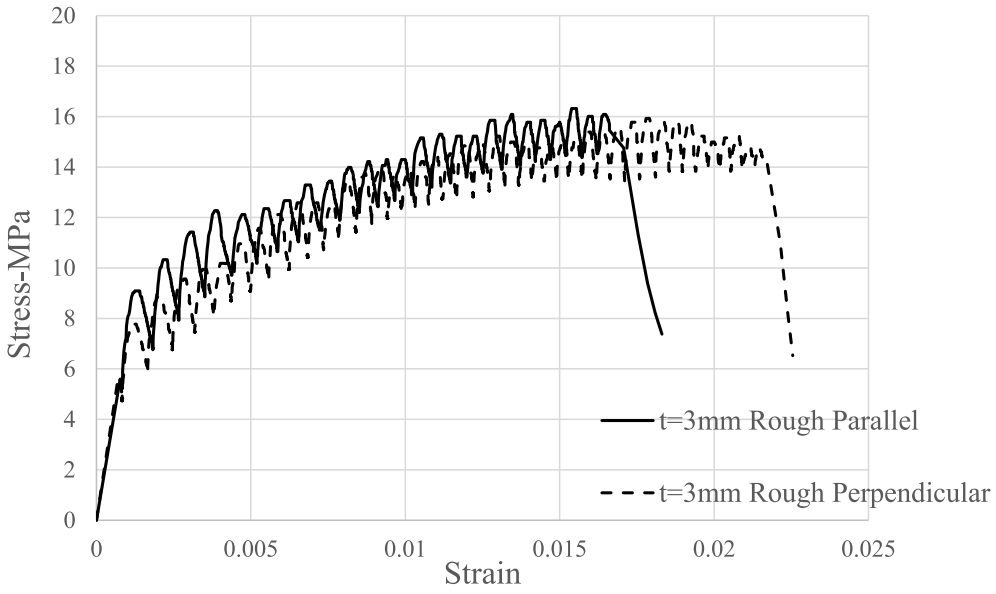

Fig. 6. Comparison of stress-strain response in tension for grains parallel and perpendicular to load direction. (1 MPa = 0.15 ksi).

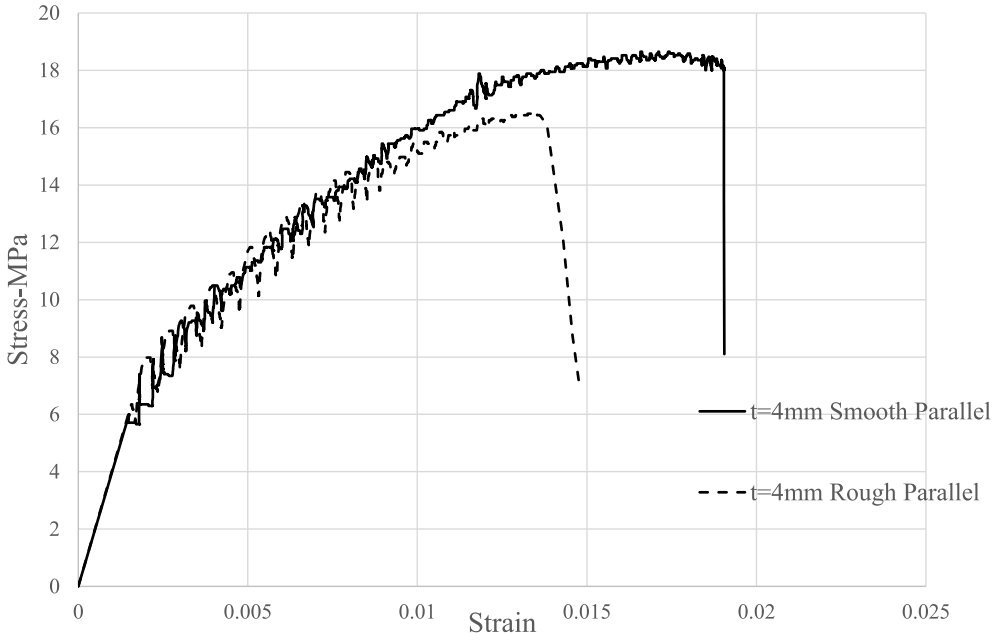

Fig. 7. Comparison of stress-strain response in tension for smooth and rough texture surface with grains parallel to load direction (1 MPa = 0.15 ksi).

parallel grain alignments. Therefore, there was no change in the average values of the moduli of elasticity as shown in Figs. 4–6.

- For smooth surface textured material with either grain orientation, the elastic modulus increased by 6% while the inelastic modulus increased by 21% due to lower porosities of smooth surface textures. During the elastic state, the elastic modulus is not affected much by the porosity.
- The modulus of elasticity of the different types of composites presented in the literature review showed lower results in the range of 1500 MPa (225 ksi) due to the smaller quantity of fillers. For PP/$CaCO_3$ with micro fillers at 50 wt% [14] the modulus of elasticity compared well to the 3 mm (0.12 in.) thick material at 7000 MPa (1050 ksi) while for PA6/$CaCO_3$ with 20 wt% of filler [24] the values compared well with the 5 mm (0.19 in.) thick material at 3500 MPa (525 ksi).

3.5.2. *Tensile stress*

- All tensile stresses decreased with an increase in thickness due to porosity. For grains aligned with the load direction, the proportional stress σ_p decreased from 18 MPa (2.7 ksi) to 2.75 MPa (0.41 ksi), the ultimate stress σ_u decreased from 27.4 MPa (4.11 ksi) to 14.03 MPa (2.1 ksi), and the rupture stress σ_r decreased from 14 MPa (2.1 ksi) to 6 MPa (0.9 ksi). For thick sections, the different stresses did not vary with thickness as shown in Fig. 4. The high value of ultimate stress for thin sections (low porosity) is due to the viscoelastic mechanism as shown in Figs. 4 and 5 were a rebound of stress occurs for each corresponding strain until reaching ultimate state where failure is localized at a specific location along the specimen.
- For grains perpendicular to the load direction, the values for proportional and rupture stress averaged almost the same value as for parallel grain alignments thus no variation with grain alignment. The

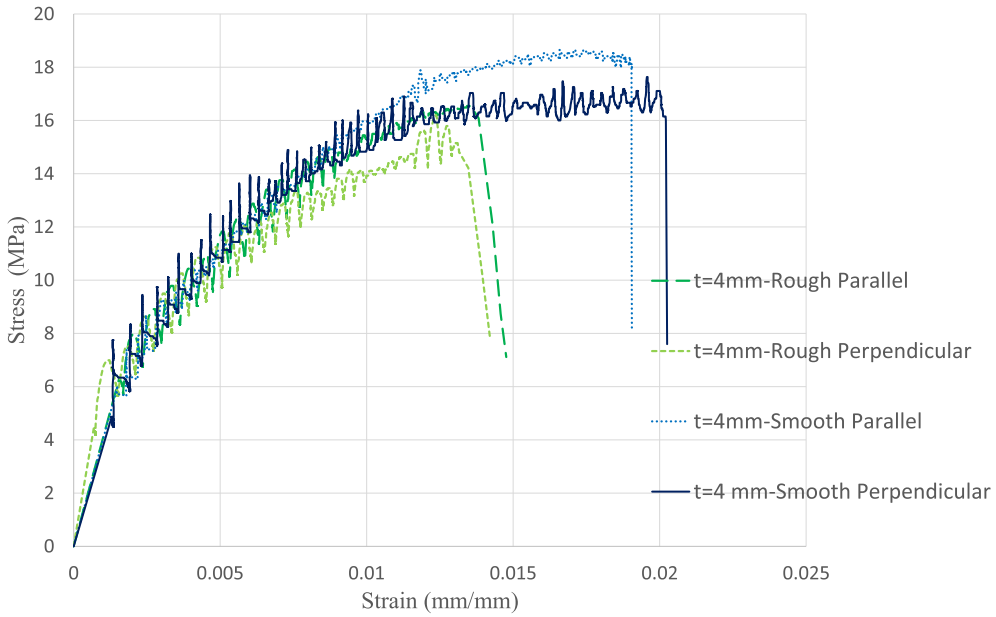

Fig. 8. Comparison of stress-strain response in tension for rough and smooth textured surfaces with grains parallel and perpendicular to load direction.(1 MPa = 0.15 ksi).

ultimate stress for thin sections with grains perpendicular to the load direction was at 22 MPa (3.3 ksi) lower than for parallel grain directions at values of 27.4 MPa (4.11 ksi). For thick sections, the value of the ultimate stress did not change with grain alignment as shown in Figs. 4 and 5 due to high porosities.

- All stresses for smooth textured samples for either grain direction increased about 16% to 18% as shown in Fig. 7.
- The tensile strengths of the different composites discussed in the literature review presented higher values ranging between 35 MPa (5.25 ksi) and 55 MPa (8.25 ksi) due to the fineness of the filler. For PP/$CaCO_3$ composites [12], the ultimate and rupture stresses at 16 MPa (2.4 ksi) and 3.4 MPa (0.51 ksi) were close to the obtained values for thick sections due to the same filler size. HDPE/$CaCO_3$ composites [17] with ultimate and rupture stresses at 24 MPa (3.6 ksi) and 14 MPa (2.1 ksi) were slightly higher than the composite with thin sections since HDPE has slightly improved mechanical properties over PVC.

3.5.3. Tensile strains

- Proportional strains ε_p for grains parallel to the load direction are equal to 0.001 and are independent of the thickness. The ultimate strain ε_u and rupture strain ε_r increases from 0.01 to 0.02 as shown in Table 1 and remain constant at 0.02 for thick sections. Due to the viscoelastic mechanism and the sudden increase in ultimate stress, a deviation in the ultimate and rupture strain values between thin and thick sections are noted as shown in Figs. 4 and 5.
- Strains vary insignificantly with grain orientation when comparing results in Tables 1 and 2 and as shown in Fig. 8. However Fig. 6 shows a slight variation in rupture strains due to some experimental errors.
- For smooth textured surfaces, the proportional strains do not change however the ultimate strains increase by 24% and the rupture strains increase by 45% which represent an improvement in ductility as shown in Fig. 8.
- Very limited information in the literature review was presented on the value of strains at break. The rupture strains of similar composites had larger values greater than 1 due to the presence of less quantities of fillers resulting in higher flexibility. For PVC/$CaCO_3$ [2, 4–7], PP/calcium carbonate composites [12,13] rubber/$CaCO_3$ [18–20], and PP/SiO_2 [15] rupture strains were higher than the obtained results for the composite ranging in values between 1 and 7. Other literature for HDPE/calcium carbonates [17] presented values at 0.1 which were more comparable and slightly higher than the values for the composite in this study due to the higher flexibility of HDPE.

3.5.4. Tensile toughness

- Toughness is a function of ultimate stress and rupture strains. Since the ultimate stresses decrease while the rupture strains increase with thickness, a slight decrease in toughness occurs with an increase in thickness. Toughness decreases from 0.23 MPa (0.035 ksi) to 0.13 MPa (0.02 ksi) for grains parallel to the load direction as shown in Table 1. The toughness value does not vary with thickness for thick sections.
- A decrease of about 13% was noted for grains perpendicular to the load direction this is due to a decrease in ultimate stress while strains are not varied. This decrease is applicable only to thin sections with an insignificant change for thick sections as shown in Tables 1 and 2.
- A 79% increase in toughness is noted for smooth textured surfaces for either grain direction resulting in higher energy absorption as shown in Fig. 8.
- Very limited information in the literature review was presented on the value of toughness. The toughness of similar composites were higher due to the larger tensile strength and rupture strain values. PP/$CaCO_3$ and HDPE/$CaCO_3$ [12,17] have toughness values of 1.9 MPa (0.285 ksi) and 1.1 MPa (0.165 ksi) respectively which are slightly higher than that for the composite in this study due to the higher flexibility of the resin. Other studies for PP/$CaCO_3$ and PP/SiO_2 composites [13,15] presented contradictory results with higher toughness values at 4.5 MPa (0.675 ksi) and 20 MPa (3 ksi) due to the presence of smaller quantities of smaller size particles in the composite.

4. Analytical modeling

In principal, the goal of analytical modeling is to develop the tensile properties and stress strain curve as a function of thickness, grain orientation and surface texture. The material tensile response is essential

in establishing the overall structural design of retrofitted structural members (this development is part of an ongoing investigation) which includes retrofitting of beams, slabs, columns and retaining walls.

4.1. Stress strain curve model

The stress stain model is presented by the following equations for each region as defined previously and as shown in Fig. 2.

- Region 1: The equation in this region is a straight line and represents the linear behavior in tension

$$\sigma = E_{el}\varepsilon \quad for \quad 0 < \varepsilon < \varepsilon_p \tag{27}$$

where σ and ε are the general stress and strain and all other parameters are as defined previously.

- Region 2: The equation in this region is a quadratic equation and represents the inelastic behavior in tension. A viscoelastic mechanism occurs for thin sections and a non-viscoelastic behavior for thick sections.

$$\sigma = A\varepsilon^2 + B\varepsilon + C \quad for \quad \varepsilon_p < \varepsilon < \varepsilon_u \tag{28}$$

$$A = \frac{\sigma_u - \sigma_p - E_{iel}(\varepsilon_u - \varepsilon_p)}{(\varepsilon_u - \varepsilon_p)^2} \tag{29}$$

$$B = E_{iel} - 2\varepsilon_p\left[\frac{\sigma_u - \sigma_p - E_{iel}(\varepsilon_u - \varepsilon_p)}{(\varepsilon_u - \varepsilon_p)^2}\right] \tag{30}$$

$$C = \sigma_u - \left[\frac{\sigma_u - \sigma_p - E_{iel}(\varepsilon_u - \varepsilon_p)}{(\varepsilon_u - \varepsilon_p)^2}\right]\varepsilon_u^2 - \left\{E_{iel} - 2\varepsilon_p\left[\frac{\sigma_u - \sigma_p - E_{iel}(\varepsilon_u - \varepsilon_p)}{(\varepsilon_u - \varepsilon_p)^2}\right]\right\}\varepsilon_u \tag{31}$$

A, B and C are constants obtained by imposing the three boundary conditions and substituting in equation (8): ($\sigma = \sigma_u$ and $\varepsilon = \varepsilon_u$), ($\sigma = \sigma_p$ and $\varepsilon = \varepsilon_p$) and ($\frac{d\sigma}{d\varepsilon}(@\varepsilon_p) = E_{iel}$)

All parameters are as defined previously. As stated previously, the stress in that region for thin sections is considered to be the average value of the extension and relaxation stress at a specific strain.

- Region 3: This equation in this region is a straight line equation between ultimate and rupture representing the descending part of the stress-stain curve. In this region the deformation is localized within the first crack region and splitting failure occurs at that location.

$$\sigma = \sigma_u + \frac{(\sigma_r - \sigma_u)}{(\varepsilon_r - \varepsilon_u)}(\varepsilon - \varepsilon_u) \quad for \quad \varepsilon_u < \varepsilon < \varepsilon_r \tag{32}$$

4.2. Properties as a function of thickness (thickness design option)

Tensile properties can be determined using empirical equations as a function of thickness based on the experimental data for grains parallel and perpendicular to the load direction. Consequently; the stress strain curve can be obtained for any specific thickness.

4.2.1. Grains parallel to the load direction

$$X_R = \frac{\gamma_1}{t^2} + \frac{\alpha_1}{t} + \beta_1 \tag{33}$$

where X_R represents the material property for a rough surface texture with grains parallel to the load direction, t is the thickness and γ_1, α_1 and β_1 are the regression line constants. β_1 represents the minimum or maximum expected tensile parameter for any thickness of material. The subscript 1 represents grains parallel to the load direction.

4.2.2. Grains perpendicular to the load direction

$$X_R = \frac{\gamma_2}{t^2} + \frac{\alpha_2}{t} + \beta_2 \tag{34}$$

where X_R represents the material property for a rough surface texture with grains perpendicular to load direction and γ_2, α_2 and β_2 are the regression line constants. β_2 represents the minimum or maximum expected property for any thickness of material. The subscript 2 represents grains perpendicular to the load direction.

4.3. Properties as a function of ultimate strength (ultimate strength design option)

Tensile properties can be determined using empirical equations as a function of ultimate strength based on the experimental data for grains parallel and perpendicular to the load direction. Consequently; the stress strain curve can be obtained for any specific strength. Equations (33) and (34) cannot be used in this case and additional empirical equations are developed.

4.3.1. Grains parallel to the load direction

$$X_R = \kappa_1\sigma_u^2 + \phi_1\sigma_u - \omega_1 \tag{35}$$

Equations (36) and (37) are used to determine the corresponding thickness for grains parallel to the load direction as a function of a specific strength for metric and US units. These equations are based on a regression analysis of thickness versus strength.

$$t = \frac{14.2}{(\sigma_u - 12.8)} \quad SI \ \ Units \tag{36}$$

$$t = \frac{0.079}{(\sigma_u - 1.92)} \quad US \ \ Units \tag{37}$$

where X_R represents the material property for a rough surface texture with grains parallel to the load direction and κ_1, ϕ_1 and ω_1 are the regression line constants. Solving equation (35) when $X_R = 0$ determines the minimum expected ultimate strength of the material with grains parallel to the load direction.

4.3.2. Grains perpendicular to the load direction

$$X_R = \kappa_2\sigma_u^2 + \phi_2\sigma_u - \omega_2 \tag{38}$$

Equations (39) and (40) are used to determine the corresponding thickness for grains perpendicular to the load direction as a function of a specific strength for metric and US units. These equations are based on a regression analysis of thickness versus strength.

$$t = \frac{8.66}{(\sigma_u - 13.54)} \quad SI \ \ Units \tag{39}$$

$$t = \frac{0.048}{(\sigma_u - 2.03)} \quad US \ \ Units \tag{40}$$

where X_R represents the material property for a rough surface texture with grains perpendicular to the load direction and κ_2, ϕ_2 and ω_2 are the regression line constants. Solving equation (38) when $X_R = 0$ determines the minimum expected ultimate strength of the material with grain perpendicular to the load direction.

4.4. Properties as a function of surface texture

The properties of smooth textured material for either design option or grain orientation are presented as a function of the same smoothness factor s_f and the corresponding rough surface material property.

Table 5
Empirical constants for properties as a function of thickness (1 N/mm = 0.0056 kip/in., 1 mm = 0.039 in., 1 MPa = 0.15 ksi, 1 N = 0.000225 kip, 1 mm^2 = 0.0015 $in.^2$).

X_R	γ_1	α_1	β_1	γ_2	α_2	β_2	s_f
E_{el}	0 N (0 kip)	18065 N/mm (101.2 kip/in.)	1013 MPa (151.9 ksi)	0 N (0 kip)	16269 N/mm (91.1 kip/in.)	987 MPa (148.1 ksi)	1.03
σ_p	0 N (0 kip)	16 N/mm (0.0896 kip/in.)	1.87 MPa (0.28 ksi)	0 N (0 kip)	15.4 N/mm (0.0862 kip/in.)	2.21 MPa (0.33 ksi)	1.14
ε_p	0 mm^2 (0 $in.^2$)	0 mm (0 in.)	0.0012	0 mm^2 (0 $in.^2$)	0 mm (0 in.)	0.0012	1.16
σ_u	0 N (0 kip)	13.7 N/mm (0.0767 kip/in.)	13.7 MPa (2.06 ksi)	0 N (0 kip)	7.77 N/mm (0.0435 kip/in.)	14.4 MPa (2.16 ksi)	1.18
ε_u	0 mm^2 (0 $in.^2$)	−0.0087 mm (-0.00034 in.)	0.0187	0 mm^2 (0 $in.^2$)	−0.014 mm (-0.00055 in.)	0.02	1.23
σ_{int}	0 N (0 kip)	14.1 N/mm (0.0789 kip/in.)	1.16 MPa (0.174 ksi)	0 N (0 kip)	13.7 N/mm (0.0767 kip/in.)	0.88 MPa (0.132 ksi)	1.06
E_{iel}	0 N (0 kip)	2353 N/mm (13.18 kip/in.)	493.4 MPa (74.01 ksi)	0 N (0 kip)	2007.9 N/mm (11.24 kip/in.)	484.4 MPa (72.66 ksi)	1.21
σ_r	0 N (0 kip)	8.25 N/mm (0.0462 kip/in.)	5.79 MPa (0.87 ksi)	0 N (0 kip)	7.19 N/mm (0.04 kip/in.)	5.56 MPa (0.834 ksi)	1.16
ε_r	0 mm^2 (0 $in.^2$)	−0.01 mm (-0.00039 in.)	0.02	0 mm^2 (0 $in.^2$)	−0.01 mm (-0.0039 in.)	0.022	1.45
T	0.012 N (0.0000027 kip)	0.057 N/mm (0.00032 kip/in.)	0.16 MPa (0.024 ksi)	0.01 N (0.0000027 kip)	0.027 N/mm (0.00015 kip/in.)	0.16 MPa (0.024 ksi)	1.79
TI	−0.117 mm^2 (-0.000176 $in.^2$)	1.54 mm (0.06 in.)	2.95	0.013 N (0.0000029 kip)	1.16 mm (0.045 in.)	4.21	1.79

Table 6
Empirical constants for properties as a function of ultimate strength (1 MPa^{-1} = 6.67 ksi^{-1}, 1 MPa = 0.15 ksi, 1 MPa^{-2} = 44.5 ksi^{-1}).

X_R	κ_1	ϕ_1	ω_1	R_1^2	κ_2	ϕ_2	ω_2	R_2^2	s_f
E_{el}	0 MPa^{-1} (0 ksi^{-1})	1490.1	19118 MPa (2868 ksi)	0.65	0 MPa^{-1} (0 ksi^{-1})	1547.3	20098 MPa (3014.7 ksi)	0.36	1.03
σ_p	0 MPa^{-1} (0 ksi^{-1})	0.979	10.5 MPa (1.58 ksi)	0.75	0 MPa^{-1} (0 ksi^{-1})	1.22	14.63 MPa (2.19 ksi)	0.5	1.14
ε_p	0 MPa^{-2} (0 ksi^{-2})	0 MPa^{-1} (0 ksi^{-1})	0.0012	0.003	0 MPa^{-2} (0 ksi^{-2})	0 MPa^{-1} (0 ksi^{-1})	0.0012	0.0001	1.16
σ_u	-	–	–	–	–	–	–	–	1.18
ε_u	0 MPa^{-2} (0 ksi^{-2})	−0.0002 MPa^{-1} (-0.0013 ksi^{-1})	0.016	0.02	0 MPa^{-2} (0 ksi^{-2})	−0.0006 MPa^{-1} (-0.004 ksi^{-1})	0.02	0.1	1.23
σ_{int}	0 MPa^{-1} (0 ksi^{-1})	0.845	9.839 MPa (1.48 ksi)	0.72	0 MPa^{-1} (0 ksi^{-1})	1.0	12.25 MPa (1.84 ksi)	0.47	1.06
E_{iel}	0 MPa^{-1} (0 ksi^{-1})	131.91	953.11 MPa (142.9 ksi)	0.45	0 MPa^{-1} (0 ksi^{-1})	136.8	1324.2 MPa (198.6 ksi)	0.3	1.21
σ_r	0 MPa^{-1} (0 ksi^{-1})	0.4885	0.44 MPa (0.066 ksi)	0.789	0 MPa^{-1} (0 ksi^{-1})	0.682	3.73 MPa (0.56 ksi)	0.77	1.16
ε_r	0 MPa^{-2} (0 ksi^{-2})	−0.0003 MPa^{-1} (-0.002 ksi^{-1})	0.017	0.05	0 MPa^{-2} (0 ksi^{-2})	−0.0006 MPa^{-1} (-0.004 ksi^{-1})	0.020	0.07	1.45
T	−0.0002 MPa^{-1} (-0.001 ksi^{-1})	0.0134	0.0097 MPa (0.0015 ksi)	0.2	0.0006 MPa^{-1} (0.004 ksi^{-1})	−0.0186	0.3052 MPa (0.046 ksi)	0.055	1.79
TI	−0.0033 MPa^{-2} (-0.147 ksi^{-2})	0.2558 MPa^{-1} (1.71 ksi^{-1})	0.1419	0.18	0.0437 MPa^{-2} (1.94 ksi^{-2})	−1.455 MPa^{-1} (-9.70 ksi^{-1})	−16.091	0.141	1.79

4.4.1. Grains parallel or perpendicular to the load direction

$$X_S = X_R s_f \tag{41}$$

where X_R is the material property for rough texture with grains parallel or perpendicular to the load direction obtained from either equations (33) and (34) or (35) and (38) depending whether based on thickness design or ultimate strength design. X_S is the corresponding smooth surface textured material with grains parallel or perpendicular to the load direction. s_f is the smoothness factor for each specific property obtained from experimental data.

4.5. Analytical results and discussions

Discussions in this part of the paper focus on the empirical equations for the stress-strain response of smooth and rough surface textured composites for both parallel and perpendicular grain orientations. Tables 5 and 6 represent the empirical constants and smoothness factors used in the equations for either design options that have been developed using regression analyses based on the experimental data. Figs. 9–11 show empirical equations for the ultimate stress, rupture strain and toughness for grains parallel to the load direction as a function of its thickness. Figs. 12–15 show comparison of the empirical equations for ultimate stress, elastic modulus, and rupture stress and strain between parallel and perpendicular grain directions. Figs. 16 and 17 show empirical equations for elastic modulus and toughness as a function of ultimate stress for both grain alignments. Figs. 18–20 shows typical empirical stress-strain curves as compared to experimentally developed curves.

4.5.1. Effect of thickness (thickness design option)

This is the case of a thickness design requirement. All properties except for strains decrease with an increase in thickness as shown in Figs. 9 and 10 for the typical ultimate stress and toughness. Thicker sections increase the porosity and thus lower material properties. The parameters β_1 and β_2 in equations (33) and (34) are shown in Table 6 and they represent the minimum or maximum values that can be attained for each property for grains parallel and perpendicular

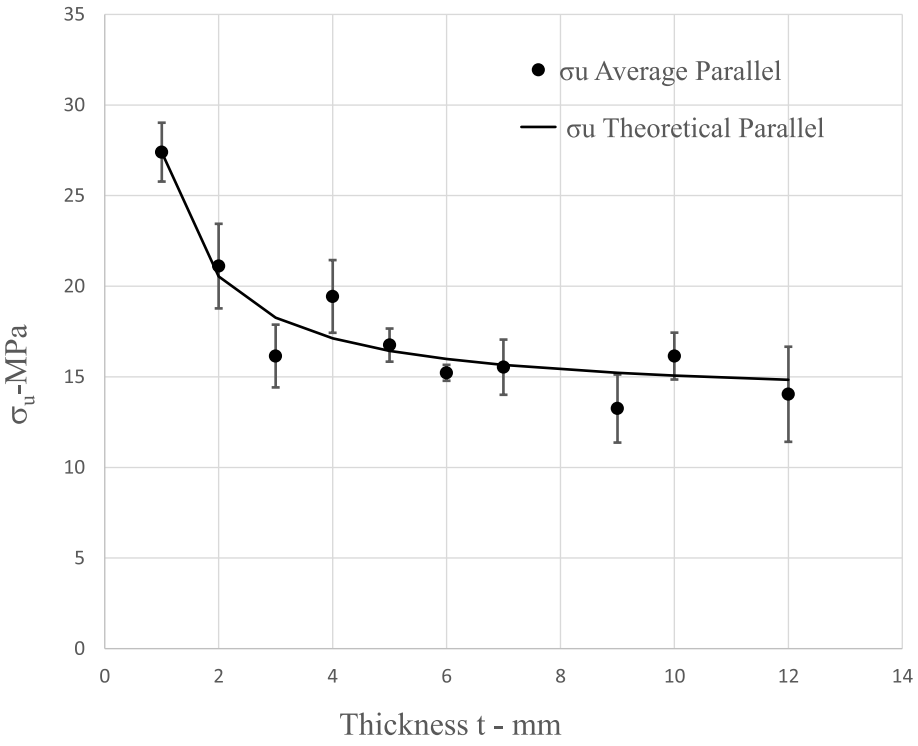

Fig. 9. Ultimate stress in tension for grains parallel to load direction as a function of thickness. (1 MPa = 0.15 ksi, 1 mm = 0.039 in.). (Error bars based on ± 1 standard deviation).

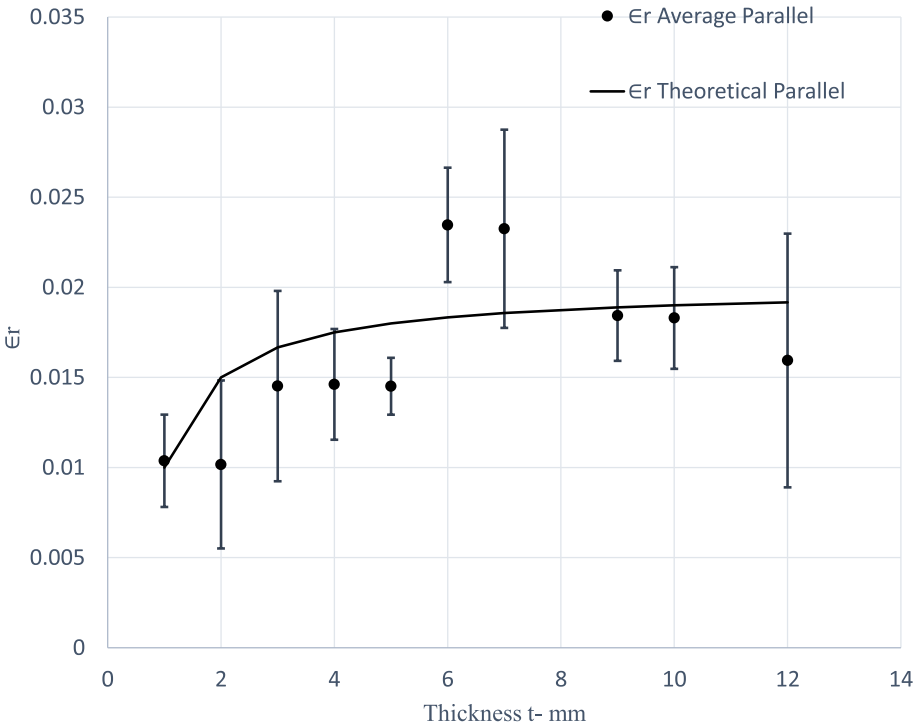

Fig. 10. Rupture strain in tension for grains parallel to load direction as a function of thickness. (1 mm = 0.039 in.). (Error bars based on ± 1 standard deviation).

respectively. As noted from the Figs. 9 and 11, material properties decrease sharply at low thickness and tend to level out as the thickness increases. Proportional strains do not vary with thickness. Ultimate and rupture strains increase sharply at low thicknesses and tend to level out for thick sections as shown in Fig. 11 for rupture strains.

4.5.2. Effect of ultimate strength (ultimate design option)

This is the case of tensile ultimate strength design requirements. The relationship between the material properties and ultimate strength is linear for all material properties except for toughness and toughness index. Figs. 16 and 17 show the relationship between the elastic modulus of elasticity and toughness as a function of ultimate stress. In

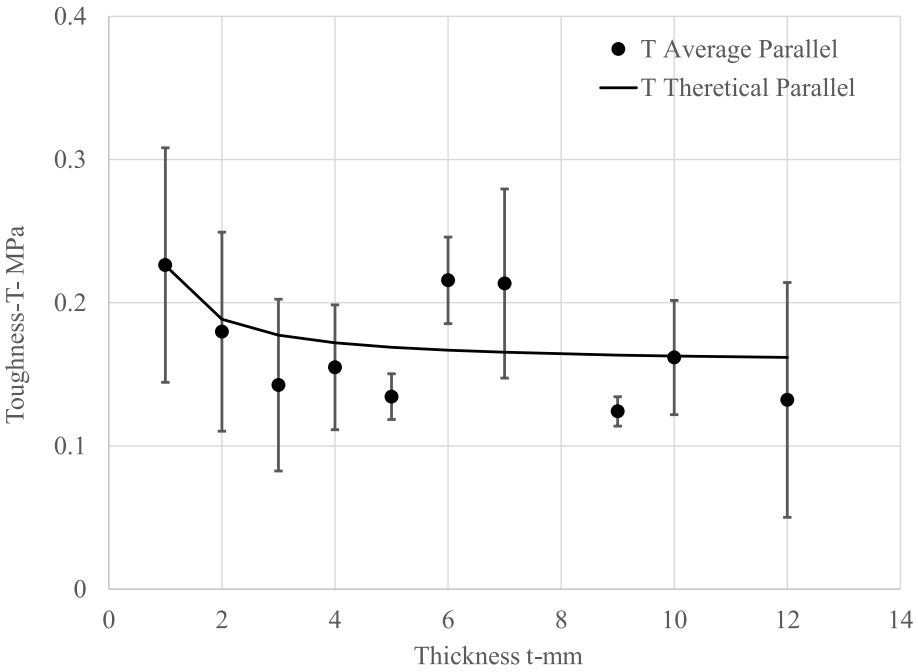

Fig. 11. Toughness in tension for grains parallel to load direction as a function of thickness (1 MPa = 0.15 ksi, 1 mm = 0.039 in.). (Error bars based on ± 1 standard deviation).

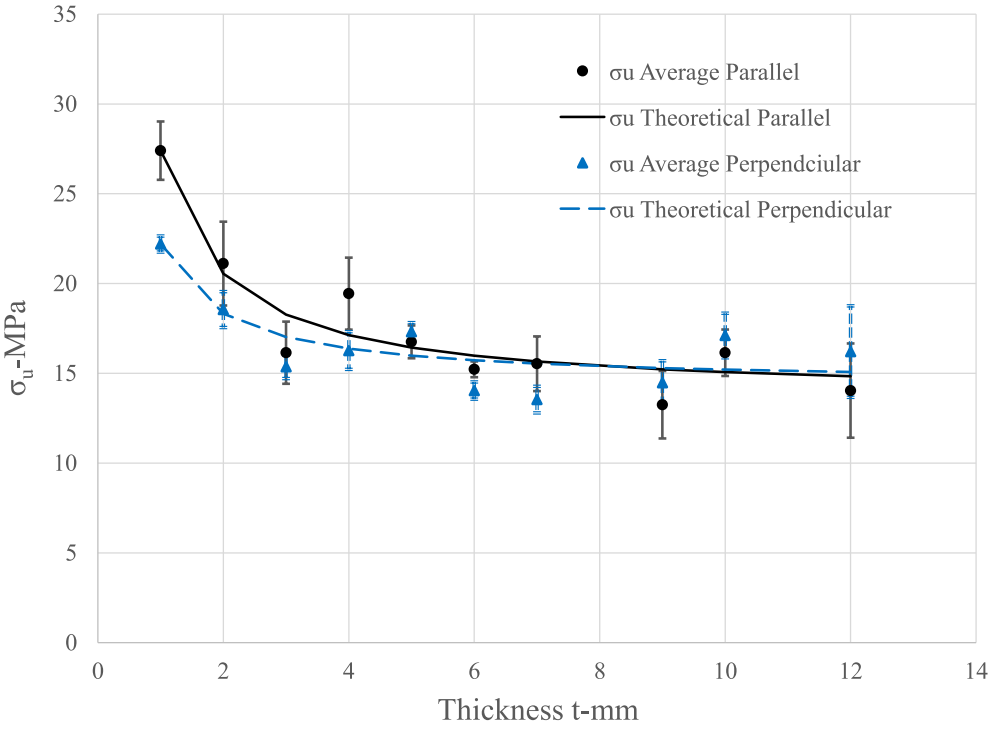

Fig. 12. Comparison of ultimate stress in tension for grains parallel and perpendicular to load direction as a function of thickness. (1 MPa = 0.15 ksi, 1 mm = 0.039 in.) (Error bars based on ± 1 standard deviation).

Fig. 16, a scatter in the data is noted at high ultimate strengths for thin sections due to the inaccurate calculations of ultimate stress for the viscoelastic behavior while the data converges for typical thicker thicknesses (satisfactory value of $R^2 = 0.6$). Solving equations (35) and (38) for ultimate strength when $X_R = 0$ for all the different properties in Table 6, leads to a minimum value of ultimate strength for parallel or perpendicular grain orientation. The values in Table 6 for κ_2, ω_2 and ϕ_2 are different than κ_1, ω_1 and ϕ_1 since equations (35) and (38) are a function of ultimate stress which is different for parallel and perpendicular grain orientations. In the case of ultimate stress design one cannot use the value of t from equations (36) and (37) or (39) and (40) and back substitute into equations (33) or (34) to obtain values for the properties because the equations are empirical and not analytical (i.e. obtained from regression analyses). Fig. 16 shows results for the toughness with grains perpendicular to the load direction as a function of ultimate strength. The trend is parabolic since toughness is the area

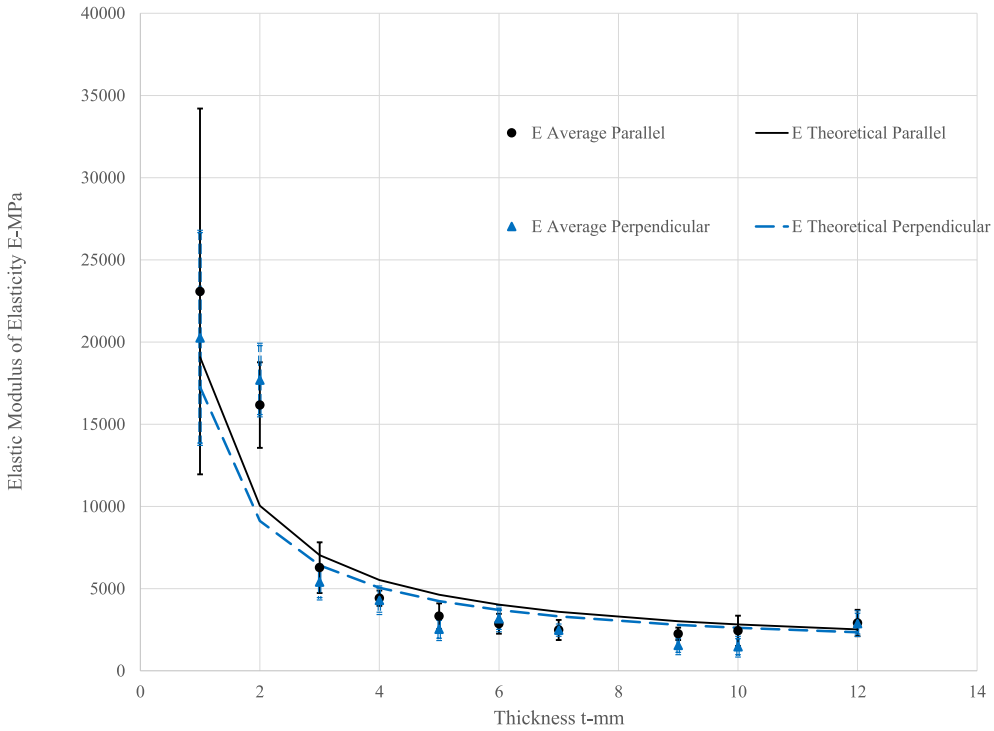

Fig. 13. Comparison of modulus of elasticity in tension for grains parallel and perpendicular to load direction as a function of thickness (1 MPa = 0.15 ksi, 1 mm = 0.039 in.). (Error bars based on ± 1 standard deviation).

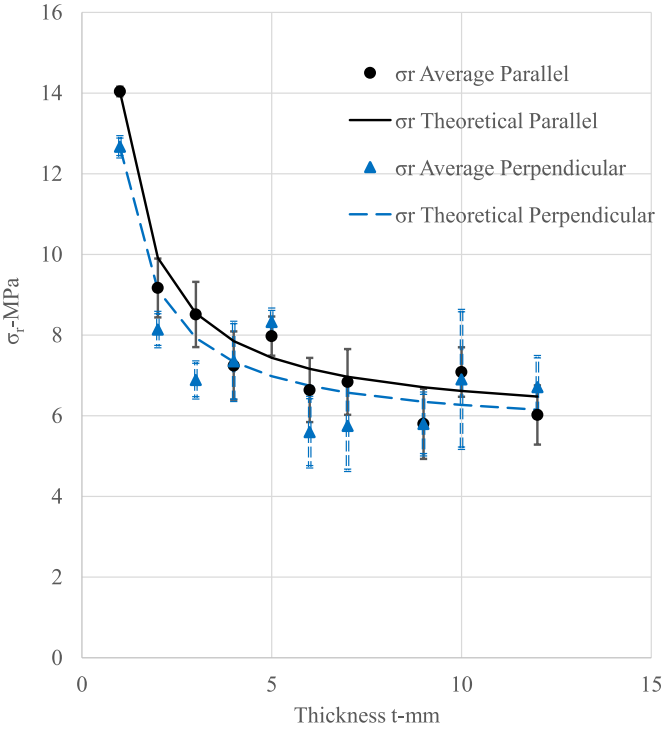

Fig. 14. Comparison of rupture stress in tension for grains parallel and perpendicular to load direction as a function of thickness (1 MPa = 0.15 ksi, 1 mm = 0.039 in.). (Error bars based on ± 1 standard deviation).

under the stress strain curve which is the product of two parameters each varying linearly with ultimate strength. The data also shows a relatively wide spread scatter of values for perpendicular grain orientation (low value of $R^2 = 0.055$) due to the variation in the material production, grain orientation and inaccurate calculation of the area under the stress strain curves in particular for thin sections due to the viscoelastic mechanism.

4.5.3. *Effect of grain orientation*

The ultimate stress, toughness and toughness index are the only parameters affected by the grain orientation. Fig. 12 shows a deviation of ultimate stress at lower thickness between the different grain orientations however the variation tends to decrease as thickness increases. Other parameters as shown in Figs. 13–15 for the modulus of elasticity, rupture stress and strain show insignificant variation due to grain orientation. As shown in Table 5 the values for (α_1, α_2), (β_1, β_2) and (γ_1, γ_2) are close indicating that the grain orientation has no effect on the material properties for all thickness except for ultimate stress, toughness and toughness index. The values for ultimate stress of $\alpha_1 = 13.7$ N/mm (0.0767 kip/in.), $\alpha_2 = 7.77$ N/mm (0.0435 kip/in.) and for toughness $\gamma_1 = 0.012$ N (0.0000027 kip), $\alpha_1 = 0.057$ N/mm (0.00032 kip/in.), $\gamma_2 = 0.01$ N (0.0000027 kip), $\alpha_2 = 0.027$ N/mm (0.00015 kip/in.) are significantly different which implies that for thin sections both property values are lower for perpendicular grain alignments than for parallel grain alignments. However since the (β_1, β_2) values are close, this implies that ultimate stress and toughness values are not affected by grain orientation for larger thicknesses.

4.5.4. *Effect of surface texture*

The effect of surface texture is presented by the smoothness factor s_f. As shown in Tables 5 and 6 the value for smoothness factor is greater than one indicating that smooth surface materials result in improved tensile response. Moduli of elasticity, and stresses are slightly improved based on s_f values in the range of 1.16. The proportional and ultimate strains were increased by 16 and 23% respectively. As shown in Tables 5 and 6, the rupture strains were increased by 45% resulting in an increase in toughness and toughness indices of 79% thus improving energy absorption and ductility of the composite. This increase in strain is noted since porosity is affected more by the change in surface texture than by the change in thickness of the material.

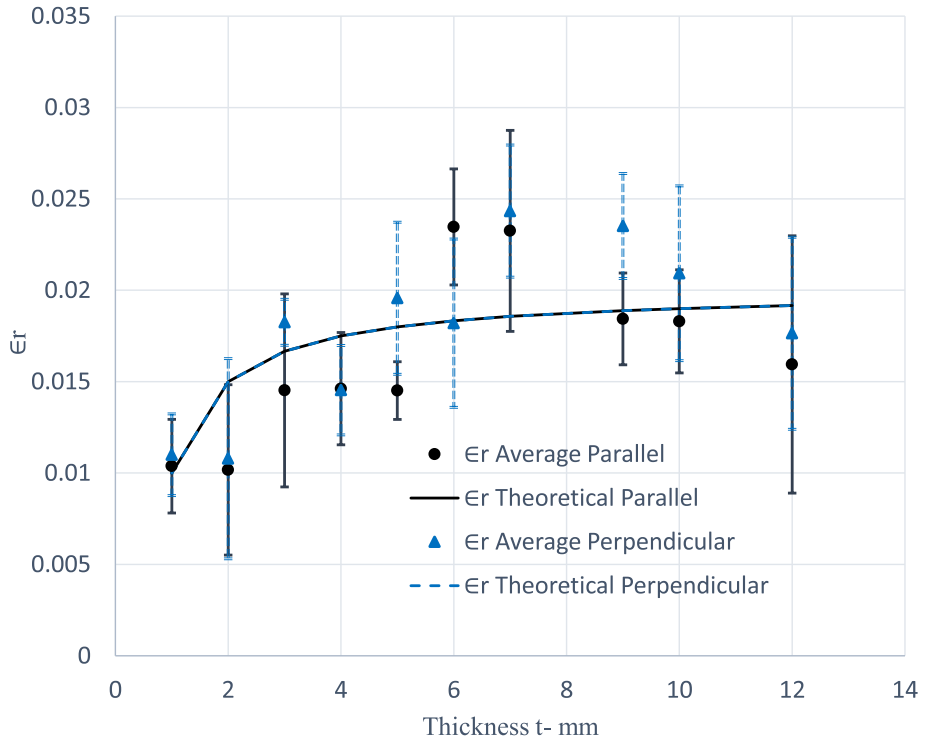

Fig. 15. Comparison of rupture strain in tension for grains parallel and perpendicular to load direction as a function of thickness (1 mm = 0.039 in.). (Error bars based on ± 1 standard deviation).

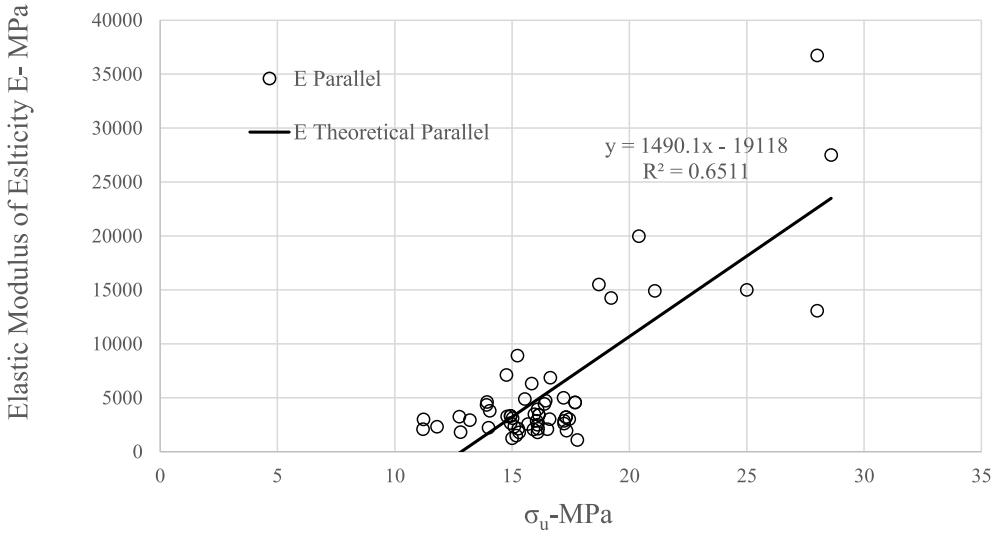

Fig. 16. Elastic modulus in tension for grains parallel to load direction as a function of σ_u. (1 MPa = 0.15 ksi).

5. Conclusions

- For different composite thicknesses ranging between 1 mm (0.039 in.) and 12 mm (0.47 in.), the maximum tensile strengths decreased from 28 MPa (4.2 ksi) to 16 MPa (2.4 ksi). The modulus of elasticity decreased from 23,078 MPa (3462 ksi) to 2139 MPa (321 ksi) resulting in an increase in ultimate and rupture strains from 0.01 to 0.02 due to lower stiffness. In addition the toughness of the material decreased from 0.23 MPa (0.035 ksi) to 0.13 MPa (0.02 ksi). The decrease in the tensile properties with thickness is due to the high porosity of the material. Tensile properties for thick sections vary insignificantly with thickness.
- The grain orientation of the material did not affect the material properties except for the ultimate strength and toughness of thin sections with a decrease of about 20% for grains perpendicular to the load direction.
- For smooth textured surface and due to low porosity, the stresses and moduli of elasticity increased by about 16% while the strains at peak and rupture increased by 45% which led to an increase in toughness about 79%. The smoothness of the surface texture resulted in greater improvement of ductility and energy absorption.
- When comparing to similar composites, thin sections of the composite have a viscoelastic behavior with load extension and release in the ascending portion of the stress-strain curve which is essential for achieving durability, higher strengths, higher energy absorption and

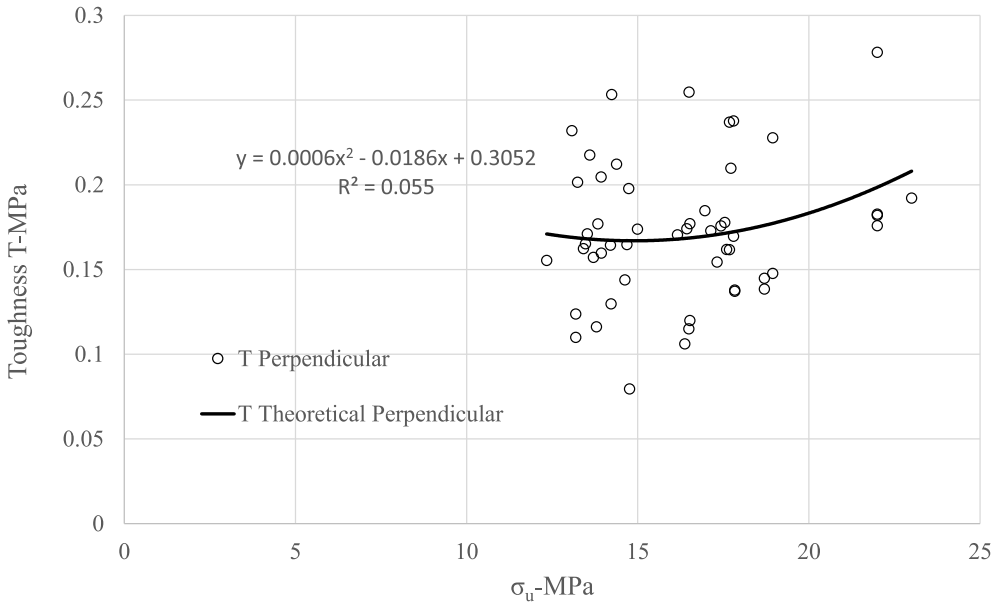

Fig. 17. Toughness in tension for grains perpendicular to load direction as a function of σ_u (1 MPa = 0.15 ksi).

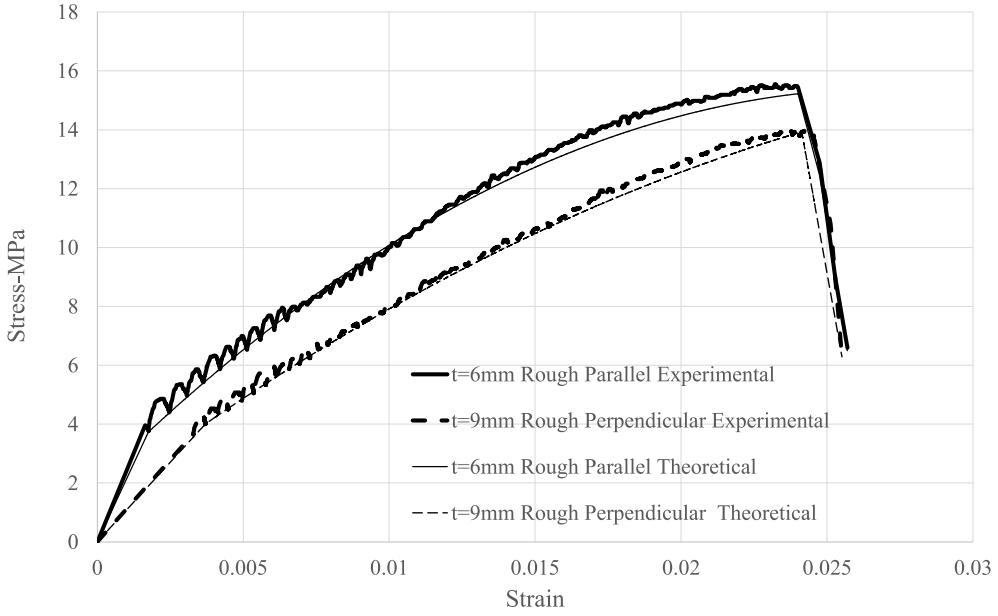

Fig. 18. Experimental and theoretical stress strain curves in tension for rough texture with grains parallel and perpendicular to load direction for 6 mm and 9 mm thicknesses (1 MPa = 0.15 ksi, 1 mm = 0.039 in.).

ductility. The tensile mechanical properties are dependent on the size and quantity of particles in the composite which indirectly affects the porosity and flexibility. The composite in this study has larger quantities of larger size particles in order to preserve the rigidity for retrofit applications however resulting in relatively lower strengths, toughness and rupture strains compared to similar composites. The moduli of elasticity of thick materials were slightly higher than similar composites due to the material rigidity (larger quantity of fillers) however the values are still lower compared to cementitious and polymer composites which is beneficial for seismic and blast retrofits [41,42].

- Another benefit of the tensile response of this composite is its delayed strength resulting in higher stresses at large rupture strains which is beneficial for resisting nonconventional loads such as impact and blast [41,42].
- The developed analytical models for the stress strain curves and mechanical properties as a function of grain alignment, thickness and surface texture compared well with the obtained experimental data. However some of the experimental data for toughness and strains show a wide scatter beyond mean values due to the variation in the manufacturing process of the material planks.
- The derived tensile stress strain models shall be used when designing structural elements retrofitted with PVC/$CaCO_3$ composites (i.e. when used simultaneously as formwork and additional or replacement of reinforcing bars in beams and slabs or confinement of columns).
- For retrofit, the use of calcium carbonates in PVC/$CaCO_3$ composites provides the necessary rigidity while maintaining the required tensile properties of the resin. The material is easier to handle and has great variability and flexibility in its construction application. Its

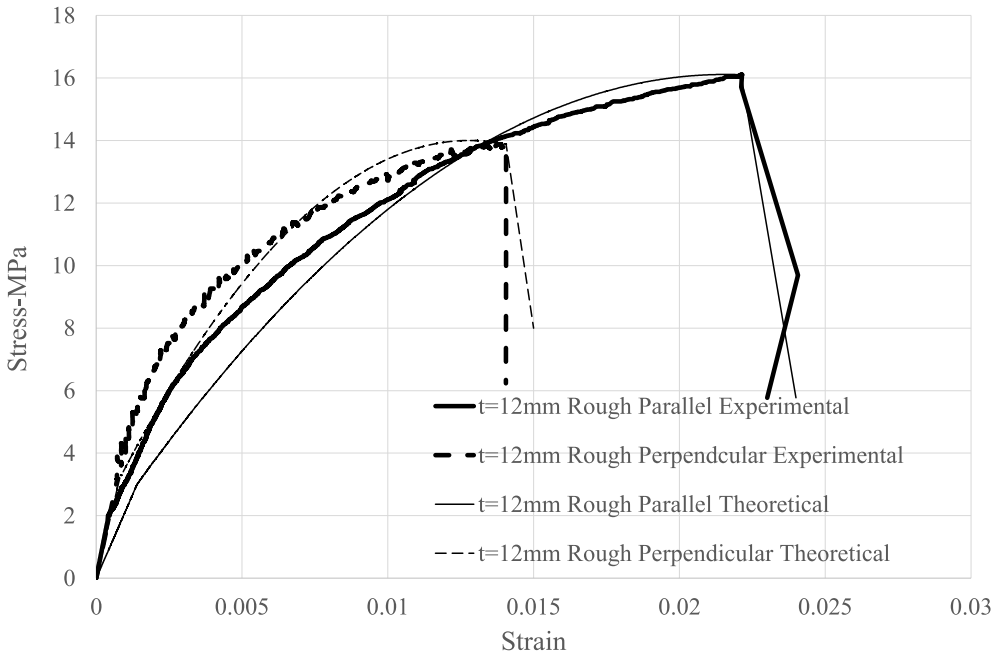

Fig. 19. Experimental and theoretical stress strain curves in tension for rough texture with grains parallel and perpendicular to load direction for 12 mm thickness (1 MPa = 0.15 ksi, 1 mm = 0.039 in.).

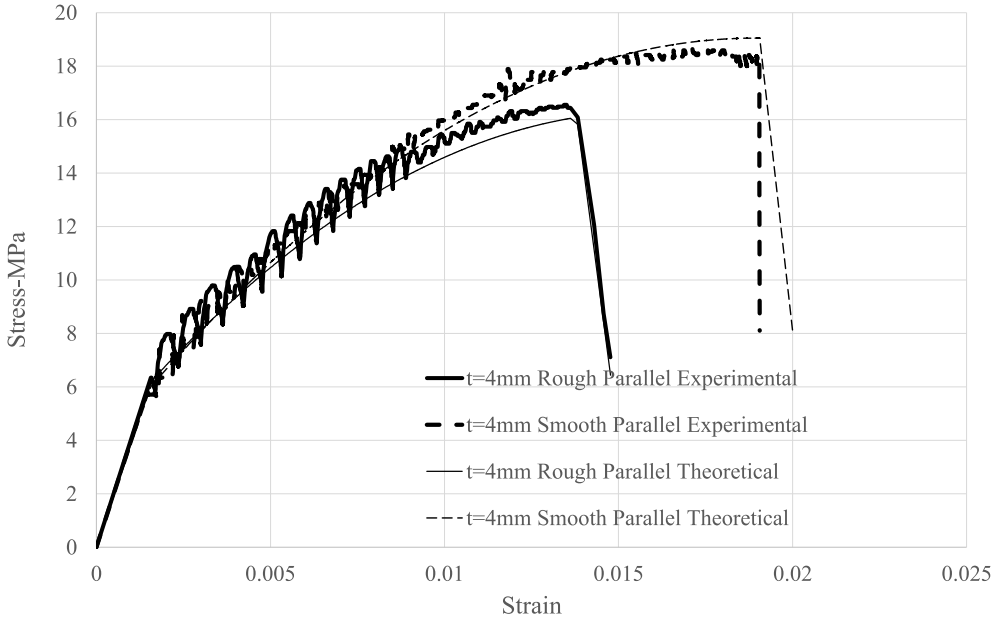

Fig. 20. Experimental and theoretical stress strain curves in tension for rough and smooth texture with grains parallel to load direction for 4 mm thickness (1 MPa = 0.15 ksi 1 mm = 0.039 in.).

benefits include its thermo-formability in addition to it being recyclable, fire/water proof, and durable. The manufacturing process of the material will allow flexibility by varying the porosity in achieving the desired tensile properties as needed for the structural retrofit application. All features including high material strength, high ductility, durability, versatility in manufacturing and construction on the field makes it a viable material for repair and retrofit. However this does not mean that it eliminates the need for other composites. Each of these materials have their specific application for which it is best suited. This material could be more suited for retrofit of beams, slabs, column or beam-column joint jacketing and not suited for zones of infill such as around reinforcing bar anchorages or infill at bridge expansion joints as achieved by cementitious composites.

- Investigation of the structural use of this material for the retrofit of beams, slabs, walls, columns and column confinement are part of an ongoing funded research. In addition, investigations are ongoing related to the effect of the variation in the percentage and size of calcium carbonate fillers on its mechanical properties as well as replacement of calcium carbonate fillers with silica sand.

Credit author statement

Sary Malak: Methodology, Validation, Formal Analysis,

Investigation, Writing-Original Draft, Writing-Review and Editing, Supervision NDU Staff: Project administration.

Declaration of competing interest

The authors declare that they have no known competing financial interests or personal relationships that could have appeared to influence the work reported in this paper.

Acknowledgement

Author would like to thank NOVAFLOOR Company for supplying the materials and for manufacturing the product. Many thanks to NDU staff, students and lab technicians who contributed with the tensile testing and results.

List of notations

The following symbols are used in this paper

α_1, α_2	empirical regression constants for grains parallel or perpendicular (thickness design)
β_1, β_2	empirical regression constants for grains parallel or perpendicular (thickness design)
C_1, C_2, C_3, C_4, C_5	proportionality constants
γ_1, γ_2	empirical regression constants for grains parallel or perpendicular (thickness design)
E	general modulus of elasticity
E_{el}	tensile elastic modulus
E_{iel}	tensile inelastic modulus
ε	general strain
ε_p	tensile proportional strain
ε_r	tensile rupture strain
ε_u	tensile ultimate strain
κ_1, κ_2	empirical regression constants for grains parallel or perpendicular (ultimate stress design)
p	porosity
S	spacing of rotating cylinders
s_f	smoothness factor
σ	general stress
σ_{int}	tensile intercept stress
σ_p	tensile proportional stress
σ_r	tensile rupture stress
σ_u	tensile ultimate strength
T	tensile toughness
T_e	heating temperature of the manufacturing process
TI	tensile toughness index
t	thickness
V	relative speed of rotating cylinders
ϕ_1, ϕ_2	empirical regression constants for grains parallel or perpendicular (ultimate stress design)
X_R	property for rough surface with grains parallel or perpendicular to load direction
X_S	property for smooth surface with grains parallel or perpendicular to load direction
ω_1, ω_2	empirical regression constants for grains parallel or perpendicular (ultimate stress design)

References

[1] Aznizam Abu Bakar, Nurul Nazihah Mohmed Rosli, Effect of nano-precipitated calcium carbonate on mechanical properties of PVC-U and PVC-U/acrylic blend, Jurnal Teknalogi 45 (F) (2006) 83–93. Dis.

[2] Xiao-Lin Xie, Qing-Xi Liu, Robert Kwok Yiu Li, Xing-Ping Zhou, Qing-Xin Zhang, Zhong-Zhen Yu, Yiu-Wing Mai, Rheological and mechanical properties of PVC/$CaCO_3$ nanocomposites prepared by in situ polymerization, Polymer 45 (2004) 6665–6673.

[3] Ning Chen, Chaoying Wan, Yong Zhang, Yinxi Zhang, Effect of nano-$CaCO_3$ on mechanical properties of PVC and PVC/Blendex blend, Polym. Test. 23 (2004) 169–174.

[4] Chuansheng Liu, Chengbao Wu, L.I.N. Lieshu, A study on the interfacial adhesion strength of different types of calcium carbonate filled poly (vinyl chloride) composites", advances in engineering research, in: 7th International Conference on Mechatronics", Control and Materials (ICMCM, vol. 104, 2016.

[5] Xuehua Chen, Chunzhong Li, Shoufang Xu, Ling Zhang, Wei Shao, H.L. Du, Interfacial adhesion and mechanical properties of PMMA-coated CaCO3 nanoparticles reinforced PVC composites", China Particuol. 4 (25–30) (2006).

[6] Irene Bonadies, Maurizio Avella, Roberto Avolio, Cosimo Carfagna, Maria Manuela Errico, Gennaro Gentile, Poly (vinyl chloride)/CaCO3 nanocomposites: influence of surface treatment on the properties, J. Appl. Polym. Sci. 122 (2011) 3590–3598.

[7] Amin Al Robaidi, Mousa Ahmad, Sami Massadeh, Ibrahim Al Rawabdeh, Nabil Anagreh, The potential of silane coated calcium carbonate on mechanical properties of rigid PVC composites for pipe manufacturing, Mater. Sci. Appl. 2 (2011) 481–485.

[8] Abeer Adnan Abd, Sudying the mechanical and electrical properties of epoxy with PVC and calcium carbonate filler, Int. J. Eng. Technol. 3 (4) (2014) 545–553.

[9] Shuisheng Sun, Chunzhong Li, Ling Zhang, H.L. Du, J.S. Burnell-Gray, Effects of surface modification of fumed silica on interfacial structures and mechanical properties of poly(vinyl chloride) composites", Eur. Polym. J. 42 (2006) 1643–1652.

[10] M.Y.A. Fuad, H. Hanim, R. Zarina, Z.A. Mohd. Ishak, Azman Hassan, Polypropylene/calcium carbonate nanocomposites-effects of processing techniques and maleated polypropylene compatibilisr, Express Polym. Lett. 4 (10) (2010) 611–620.

[11] Ming Qui Zhang, Min Zhi Rong, Shun Long Pan, Klaus Freidrich, Tensile Properties of Polypropylene filled with nanoscale calcium carbonate particles, Adv. Compos. Lett. 11 (6) (2002).

[12] Y.W. Leong, M.B. Abu Bakar, Z.A. Mohd. Ishak, A. Ariffin, B. Pukanszky, Comparison of the mechanical properties and interfacial interactions between talc, kaolin, and calcium carbonate filled polypropylene composites, J. Appl. Polym. Sci. 91 (2004) 3315–3326. March.

[13] Danil Eiras, Luiz Antonio Pessan, Mechanical properties of polypropylene/calcium carbonate nanocomposites, Mater. Res. 12 (4) (2009). Sao Carlos.

[14] Leif Jilken, Goran Malhammar, Ragnar Selden, ", The effect of mineral fillers on impact and tensile properties of polypropylene", Polym. Test. 10 (1991) 329–344.

[15] Chun Lei Wu, Ming Qiu Zhang, Min Zhi Rong, Klaus Friedrich, Tensile performance improvement of low nanoparticles filled-polypropylene composites, Compos. Sci. Technol. 62 (2002) 1327–1340.

[16] Yung Ngothai, Putra Handoko, Togay Ozbakkaloglu, Seracino Rudolf, ", Effect of $CaCO_3$ size on the mechanical properties of recycled HDPE", *Thermoplastic Polyolefin Blends*, J. Vinyl (2009). January.

[17] Z. Bartczak, A.S. Argon, R.E. Cohen, M. Weinberg, Toughness mechanism in semi-crystalline polymer blends: II. High-density polyethylene toughened with calcium carbonate filler particles, Polymer 40 (1999) 2347–2365.
[18] S. Manroshan, A. Baharin, The effect of calcium carbonate on the mechanical properties and morphology of natural rubber latex films, in: 13th Scientific Conference & 14th Annual General Meeting, Electron Microscopy Society of Malaysia, 2004, 13-15 December.
[19] N. Phuhiangpa, S. Phonghanphanee, W. Smitthipong, " Study of rubber/calcium carbonate composites", *The international Conference on Materials Research and Innovation (ICMARI)*, Mater. Sci. Eng. *773* (2020), 012013.
[20] Al-Mosawi, M.M. Ali, J.H. Mohmmed, Experimental approach to mechanical properties of natural rubber mixing with Calcium carbonate powder, Int. J. Phys. Sci. 7 (49) (30 December 2012) 6280–8282.
[21] Ligui Xiong, Zhigang Tu, Shangxian Zhang, Xiaoyuan Liu, Xingni Peng, Preparation of PBS and $CaCO_3$ composite degradable materials based on melt blending, IOP Conf. Ser. Mater. Sci. Eng. 730 (2020), 012012.
[22] S.T. Wicaksono, A.H. Laksana, Hosta Aardhyananta, ", Effect of calcium carbonate on the tensile and density properties of kenaf/polyester hybrid composite", IOP Conf. Ser. Mater. Sci. Eng. 546 (2019), 042019.
[23] Hongzhen Cai, Keyan Yang, Weiming Yi, Effects of calcium carbonate on preparation and mechanical properties of wood/plastic composite, Int. J. Agric. Biol. Eng. 10 (1) (January 2017).
[24] B.C> Bonse, L.M. Molina, Effect of calcium carbonate particle size and content on polyamide 6 processing and properties, Polym. Process. Soc. PPS 1779 (1) (2016, October) 030019-1–030019-5.
[25] Mateusz Barczewski, Marek Szostak, Marta Kulesza, Krstyna Siwak, Influence of Calcium Carbonate on Mechanical Properties and Structure of Polyurethane Composites Formed by Rotational Molding:, Conference Paper, October 2017.
[26] Ji-Zhao Liang, De-Rong Duan, Chak-Yin Tang, Chi-Pong Tsui, Da-Zhu Chen, Tensile properties of PLLA/PCL composites filled with nanometer calcium carbonate, Polym. Test. 32 (2013) 617–621.
[27] E. Guth, J. Appl. Phys. 16 (1945) 20–25.
[28] B. Pukanszky, B. Turczanyi, F. Tudos, Composites dependence of tensile yield stress in filled polymers, J. Mater. Sci. Lett. 7 (1988) 160–162.
[29] J. Jancar, J. Kucera, Yield behavior of polypropylene filled with $CaCO_3$ and $Mg(OH)_2$, I: "zero interfacial adhesion", Polym. Eng. Sci. 30 (1990) 707–713.
[30] J. Jancar, J. Kucera, Yield behavior of PP/$CaCO_3$ and $Mg(OH)_2$, II: "enhanced interfacial adhesion", Polym. Eng. Sci. 30 (1990) 714–720.
[31] M. Sumita, H. Tsukihi, K. Miyasaka, K. Ishikawa, Dynamic mechanical properties of polypropylene filled with ultrafine particles, J. Appl. Polym. Sci. 29 (1984) 1523–1530.
[32] Y.-P. Wu, Q.-X. Jia, L.-Q. Zhang, "Modeling Young's modulus of rubber-clay nanocomposites using composite theories, Polym. Test. 23 (2004) 903–909.
[33] Y. Wang, H. Shen, G. Li, K. Mai, Effect of Interfacial interaction on the crystallization and mechanical properties of PP/nano-$CaCO_3$ composites modified by compatibilizers, J. Appl. Sci. 113 (2009) 1584–1592.
[34] T.B. Lewis, L.E. Nielsen, J. Appl. Polym. Sci. 14 (1970) 1449.
[35] P.E. Padawar, N. Beecher, Polym. Eng. Sci. 10 (1970) 185.
[36] N. Nicolais, L. Nicodemo, Int. J. Polym. Mater. 3 (3) (1974) 229–243.
[37] D.M. Bigg, Polym. Compos. 8 (1987) 115–122.
[38] Z. Bartczak, A.S. Argon, R.E. Cohen, M. Weinberg, "Toughness mechanism in semi-crystalline polymer blends: I. High-density polyethylene toughened with rubbers ", Polymer 40 (1999) 2331–2346.
[39] W.-C. Huang, J. Compos. Mater. 5 (1971) 320.
[40] Zhongqiang Xiong, Yuqi Li, Lulu Pan, Jinhong Yu, Shaorong Lu, An analytical study of mechanical behavior of polypropylene/calcium carbonate composites under uniaxial tension and three point bending, Compos. Struct. 171 (2017) 370–381.
[41] S. Malak, N. Krstulovic-Opara, "Modeling Material Response of Fiber Composites Used for the Retrofit of Existing Concrete Structures under Blast Loadings "*ACI Technical Publication", Dennis Mertz Symposium on Design and Evaluation of Concrete Bridges*, 2020, pp. 114–136. SP-340-7, April.
[42] J. Conrath Edward, Krauthammer Ted, A. Marchand Kirk, F. Mlakar Paul, S.E. I. Asce, Structural Design for Physical Security State of the Practice, 1999.